

1 **Drivers of Phytoplankton Bloom Interannual Variability in the Amundsen and Pine**
2 **Island Polynyas**

3
4 **Guillaume Liniger^{1,2*}, Delphine Lannuzel^{1,3,4}, Sébastien Moreau^{5,6}, Michael S. Dinniman⁷,**
5 **Peter G. Strutton^{1,3}**

6 ¹ Institute for Marine and Antarctic Studies, University of Tasmania, Hobart, Australia

7 ² Monterey Bay Aquarium Research Institute, Moss Landing, CA, USA

8 ³ Australian Centre for Excellence in Antarctic Science, University of Tasmania, Hobart,
9 Australia

10 ⁴ Australian Antarctic Program Partnership, University of Tasmania, Hobart, Australia

11 ⁵ Norwegian Polar Institute, Tromsø, Norway

12 ⁶ iC3: Centre for ice, Cryosphere, Carbon and Climate, Department of Geosciences, UiT The
13 Arctic University of Norway, 9037 Tromsø, Norway

14 ⁷ Center for Coastal Physical Oceanography, Old Dominion University, Norfolk, VA, USA

15

16 * Corresponding Author: Guillaume Liniger (liniger@mbari.org)

17

18 **Abstract**

19 The Amundsen Sea Embayment (ASE) experiences both the highest ice shelf melt rates and the
20 highest biological productivity in West Antarctica. Using 19 years of satellite data and modelling
21 output, we investigate the long-term influence of environmental factors on the phytoplankton
22 bloom in the Amundsen Sea (ASP) and Pine Island (PIP) polynyas. We test the prevailing
23 hypothesis that changes in ice shelf melt rate could drive interannual variability in the polynyas'
24 surface chlorophyll-*a* (chl*a*) and Net Primary Productivity (NPP). We find that the interannual
25 variability and long-term change in glacial meltwater may play an important role in chl*a* variance
26 in the ASP, but not for NPP. Glacial meltwater does not explain the variability in neither chl*a* or
27 NPP in the PIP, where light and temperature are the main drivers. We attribute this to potentially
28 greater amount of iron-enriched meltwater brought to the surface by the meltwater pump

29 downstream of the PIP, and the coastal ocean circulation accumulating and transporting iron
30 towards the ASP.

31

32 **Short Summary**

33 We investigate the phytoplankton bloom variability and its drivers in the Amundsen polynyas
34 (areas of open water within sea ice). Between 1998 and 2017, we find that changes in melting ice
35 shelves may have different impacts on biological productivity between the Amundsen Sea (ASP)
36 and Pine Island (PIP) polynyas. While ice shelves melting seems to play an important role for
37 phytoplankton growth variability in the ASP, light and warmer waters appear to be more
38 important in the PIP.

39

40 **1. Introduction**

41

42 Coastal polynyas are open ocean areas formed by strong katabatic winds pushing sea ice offshore
43 (Morales Maqueda, 2004). They are the most biologically productive areas in the Southern
44 Ocean (SO) relative to their size (Arrigo et al., 1998). This high biological productivity contrasts
45 sharply with the rest of the SO, where low iron and light availability generally co-limit
46 phytoplankton growth (Boyd et al., 2007). In West Antarctica, the Amundsen Sea Embayment
47 (ASE) hosts two of the most productive Antarctic polynyas: The Pine Island Polynya (PIP) and
48 Amundsen Sea Polynya (ASP) (Arrigo and van Dijken, 2003).

49

50 The phytoplankton community in the ASE is generally dominated by *Phaeocystis antarctica*
51 (Lee et al., 2017; Yager et al., 2016), which is adapted to low iron availability and variable light
52 conditions, and forms large summer blooms (Alderkamp et al., 2012; Yager et al., 2016).

53 Diatoms like *Fragilariopsis sp.* and *Chaetoceros sp.* are also present, often becoming more
54 important near the sea-ice edge or under shallow, stratified mixed layers where silicic acid (Si)
55 and iron (Fe) are more available (Mills et al., 2012). In exceptional years, such as 2020, diatoms
56 like *Dactyliosolen tenuijunctus* replaced *P. antarctica* as the dominant taxon, driven by
57 anomalously shallow mixed layers and sufficient Fe–Si supply (Lee et al., 2022). This dynamic
58 balance highlights how light, nutrient supply, and stratification control community composition
59 in these highly productive and complex Antarctic systems.

60

61 The ASE is also the Antarctic region experiencing the highest mass loss from the Antarctic ice
62 sheet. It has been undergoing increased calving, melting, thinning and retreat over the past three
63 decades (Paolo et al., 2015; Rignot et al., 2013; Rignot et al., 2019; Shepherd et al., 2018). In the
64 ASE, this ice loss is mainly through enhanced basal melting of the ice shelves. This is attributed
65 to an increase in wind-driven Circumpolar Deep Water (CDW) fluxes and ocean heat content
66 intruding onto the continental shelf through deep troughs such as the Pine Island and Dotson-
67 Getz, and flowing into the ice shelves cavities (Dotto et al., 2019; Jacobs et al., 2011; Pritchard et
68 al., 2012). There, warm waters fuel intense basal melt of the Pine Island, Thwaites, and Getz ice
69 shelves, and returns as a fresher, colder outflow that can strengthen stratification (Jenkins et al.,
70 2010; Ha et al., 2014). The PIP and ASP differ in their exposure to CDW and in local
71 circulation: the ASP is more strongly influenced by upwelled modified CDW (mCDW) and
72 glacial meltwater inputs, whereas in the PIP, the deep mCDW retains more of its original
73 offshore characteristics, with vertical exchange only significantly occurring beneath the ice
74 shelves, leading to a more stratified and less directly ventilated surface layer (Assmann et al.,
75 2013; Dutrieux et al., 2014). These hydrographic contrasts can shape the timing and magnitude
76 of phytoplankton blooms and nutrient dynamics across the two polynyas.

77

78 Melting ice shelves can explain about 60% of the biomass variance between all Antarctic
79 polynyas, suggesting that they are the primary supplier of dissolved iron (dFe) to coastal
80 polynyas (Arrigo et al., 2015), and can directly or indirectly contribute to regional marine
81 productivity (Bhatia et al., 2013; Gerringa et al., 2012; Hawkins et al., 2014; Herraiz-
82 Borreguero et al., 2016). The strong melting of the ice shelves can release significant quantities
83 of freshwater at depth (Biddle et al., 2017), resulting in a strong overturning within the ice
84 shelves cavity, called the meltwater pump (St-Laurent et al., 2017). Modelling efforts have
85 identified both resuspended Fe-enriched sediments and CDW entrained to the surface by the
86 meltwater pump as the two primary sources of dFe to coastal polynyas, providing up to 31% of
87 the total dFe, compared to 6% for direct ice shelves input (Dinniman et al., 2020; St-Laurent et
88 al., 2017). Other drivers such as sea-ice coverage (and associated increases in light and dFe
89 availability when sea ice retreats), or winds have also been shown to impact primary productivity
90 in polynyas (Park et al., 2019; Park et al., 2017; Vaillancourt et al., 2003).

91
92 The key question of how glacial meltwater variability may impact biological productivity in the
93 ASE has previously been raised during the ASPIRE program (Yager et al., 2012). During the
94 expedition, a significant supply of melt-laden iron-enriched seawater to the central euphotic zone
95 of the ASP was observed, potentially explaining why this area is the most biologically
96 productive in Antarctica (Randall-Goodwin et al., 2015; Sherrell et al., 2015). Other studies in
97 the Western Antarctic Peninsula and East Antarctica showed that the meltwater pump process
98 was also responsible for natural Fe supply to the surface, increasing primary productivity (Cape
99 et al., 2019; Tamura et al., 2023).

100
101 In this study, we investigate the long-term relationship between the main environmental factors
102 of the ASE and the surface biological productivity, with a focus on ice shelves melting. A
103 demonstrated relationship between glacial meltwater and phytoplankton growth would have far-
104 reaching consequences for regional productivity in coastal Antarctica, and possibly offshore,
105 over the coming decades under expected climate change scenarios (Meredith et al., 2019). We
106 test the hypothesis that changes in glacial meltwater are linked to the surface ocean primary
107 productivity variability observed over the last two decades. We use a combination of satellite
108 (ocean color and ice shelf melting rate), climate re-analysis, and model data spanning 1998 to
109 2017.

110
111 **2. Material and Methods**

112
113 2.1 Study area and polynya mapping
114
115 We focus on the PIP and ASP in the ASE in West Antarctica (Fig. 1). The ASE is comprised of
116 several ice shelves and glaciers, including: Abbot (Abb), Cosgrove (Cs), Pine Island (PIG),
117 Thwaites (Tw), Crosson (Cr), Dotson (Dt) and Getz (Gt). The PIG and Thwaites have received
118 significant attention in recent years due to their potentially large contribution to sea level rise
119 (Rignot et al., 2019; Scambos et al., 2017). Along with the Crosson and Dotson ice shelves, the
120 PIG and Thwaites are undergoing the highest melt rate, which is expected to increase under
121 climate change scenarios (Naughten et al., 2023; Paolo et al., 2023). The polynyas' boundaries

were determined using a 15% sea-ice concentration (SIC) mask (Moreau et al., 2015; Stammerjohn et al., 2008) for every 8-day period from June 1998 to June 2017 to accurately represent the size of the polynyas through time.

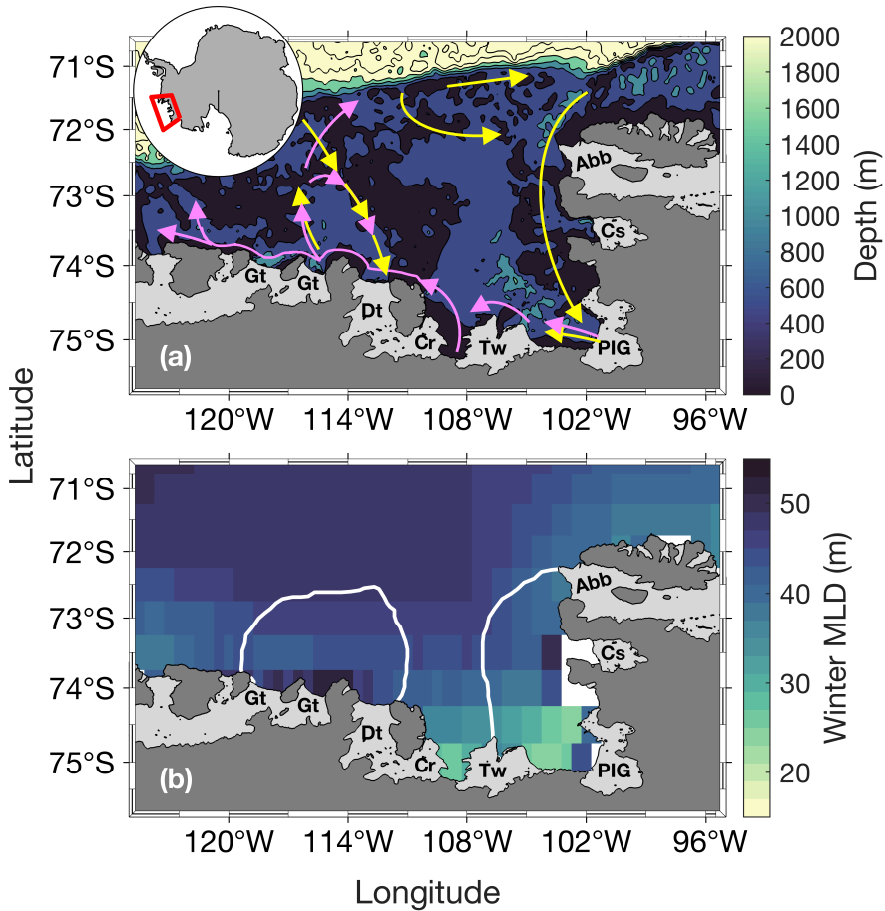


Fig. 1. Study area. Panel (a) shows the bathymetry (from ETOPO1; Amante & Eakins, 2009) and panel (b) shows the climatological April-September (that we call winter) mixed-layer depth (MLD) from 1998 to 2016 (n=114). Panel (a) shows a simplified schematic of the local deep ocean circulation (~ below 400m, yellow arrows) and upper glacial meltwater/sediments/circumpolar deep water sourced dFe pathways (magenta arrows), which follows the local upper ocean circulation. Schematic adapted from St-Laurent et al. (2017). The white lines in panel (b) represent the climatological summer polynyas' boundaries for the Amundsen (ASP; left) and Pine Island (PIP; right) polynyas. The dark grey area is mainland

152 Antarctica. Light grey areas indicate floating ice shelves and glaciers: Abbot (Abb), Cosgrove
153 (Cs), Pine Island Glacier (PIG), Thwaites (Tw), Crosson (Cr), Dotson (Dt) and Getz (Gt).

154

155 2.2 Satellite ocean surface chlorophyll-*a* and net primary productivity

156

157 We obtained level-3 satellite surface chlorophyll-*a* concentration (chl*a*) with spatial and
158 temporal resolution of 0.04° and 8 days from the European Space Agency (ESA) Globcolor
159 project. We used the CHL1-GSM (Garver-Siegel-Maritorena) (Maritorena and Siegel, 2005)
160 standard Case 1 water merged products consisting of the Sea-viewing Wide Field-of-view
161 (SeaWiFS), Medium Resolution Imaging Spectrometer (MERIS), Moderate Resolution Imaging
162 Spectroradiometer (MODIS-A) and Visible Infrared Imaging Suite sensors (VIIRS). We chose to
163 perform our analysis with the merged GlobColour product, which has been widely applied and
164 tested in Southern Ocean and coastal Antarctic studies (Ardyna et al., 2017; Sari El Dine et al.,
165 2025; Golder & Antoine, 2025; Nunes, Fereira & Brito, 2025), to increase our spatial and
166 temporal coverage.

167

168 We estimated phytoplankton bloom phenology metrics following the Kauko et al. (2021)
169 method. Firstly, for a given 8-day period, we applied a spatial 3x3 pixels median filter to reduce
170 gaps in missing data. Then, if a pixel was still empty, we applied the average chl*a* of the previous
171 and following week to fill the data gap. Data were smoothed using a 4-point moving median
172 (representing a month of data). For each pixel, the threshold for the bloom detection was based
173 on 1.05 times the annual median. The threshold method is frequently used (Racault et al., 2012;
174 Siegel et al., 2002) and proven reliable at higher latitudes (Marchese et al., 2017; Soppa et al.,
175 2016; Thomalla et al., 2023). We then determined 5 main bloom metrics. The bloom start (BS) is
176 defined as the day where chl*a* first exceeds the threshold for at least 2 consecutive 8-day periods.
177 Conversely, the bloom end is the day where chl*a* first falls below the threshold for at least 2
178 consecutive 8-day periods. The bloom duration (BD) is the time elapsed between bloom start and
179 bloom end. The bloom mean chl*a* (BM) and bloom maximum chl*a* are respectively the average
180 and maximum chl*a* value calculated during the bloom. Each year is centered around austral
181 summer, from June 10th year *n* (day 1) to June 9th year *n+1* (day 365 or 366). We also averaged
182 our 8-day data to monthly data to perform a spatial correlation analysis (see section 2.6).

183
184 We note that satellite ocean-colour chla algorithms (including the GlobColour merged product
185 used here) are globally tuned and may underperform in optically complex waters (e.g., with
186 elevated dissolved organic matter or suspended sediments, ‘Case 2’). In the ASP, past work
187 (Park et al. 2017) showed that satellite chla climatologies reflect broad seasonal patterns that are
188 consistent with *in situ* measurements of phytoplankton biomass and photophysiology, but there is
189 limited data from regions immediately adjacent to glacier fronts or during times of strong
190 meltwater input. Thus, while we consider satellite chla to be useful for capturing spatial and
191 temporal variability at polynya scale, uncertainty likely increases in optically complex zones
192 near glacier margins or during low-light periods, and needs to be considered while interpreting
193 results.

194

195 Eight-day satellite derived Net Primary Productivity (NPP) data with 1/12° spatial resolution,
196 spanning 1998 - 2017 using the Vertically Generalized Production Model (Behrenfeld and
197 Falkowski, 1997) were obtained from the Oregon State University website. The VGPM model is
198 a chlorophyll-based approach and relies on the assumption that NPP is a function of chla,
199 influenced by light availability and maximum daily net primary production within the euphotic
200 zone. SeaWiFS-based NPP data span 1998 - 2009, MODIS-based data span 2002 - 2017. To
201 increase spatial and temporal coverage, we averaged SeaWiFS and MODIS from 2002 to 2009,
202 where there was valid data for both in a pixel. NPP data were also monthly averaged and used to
203 compare with chla spatial and temporal patterns.

204

205 We caution that our study focuses on surface productivity, and satellites cannot detect under-ice
206 phytoplankton, sea-ice algal blooms, or deeper productivity, therefore likely underestimating
207 total primary productivity (Ardyna et al., 2020; Boles et al., 2020; Douglas et al., 2024; McClish
208 & Bushinsly, 2023; Stoer & Fennel 2024).

209

210 2.3 Ice shelves volume flux

211

212 We used the latest ice shelf basal melt rate estimates from Paolo et al (2023). These estimates are
213 derived from satellite radar altimetry measurements of ice shelves height, and produced on a 3

214 km grid every 3 months, with an effective resolution of ~5 km. For this study, our basal melt
215 record spans June 1998 to June 2017. We calculated ice shelves volume flux rate for every
216 gridded cell by multiplying the basal melt rate by the cell area. Data were summed for each ice
217 shelf for a 3-month period. A 5-point (15 months) running mean was applied to reduce noise,
218 such as spurious effects induced by seasonality on radar measurements over icy surfaces (Paolo
219 et al., 2016), and data were temporally averaged from October to March to match the SO
220 phytoplankton growth season (Arrigo et al., 2015), providing yearly mean values. The Abbot,
221 Cosgrove, Thwaites, PIG, Crosson, Dotson and Getz ice shelves were used to calculate a single
222 total meltwater volume flux (TVFall) for the ASE to investigate the link with surface chla and
223 NPP. We also investigated the relationship between each polynyas' productivity and their closest
224 ice shelf. The Abbot, Cosgrove, PIG and Thwaites ice shelves were used to calculate the flux
225 rate in the PIP (TVFpip) while the Thwaites, Crosson, Dotson and Getz ice shelves were chosen
226 for the ASP (TVFasp). The Thwaites was used in both due to its central position between the two
227 polynyas. We thereafter use the term glacial meltwater which defines meltwater resulting from
228 ice shelf melting.

229

230 2.4 Simulated dFe distribution

231

232 The spatial distribution of dFe from different sources in the embayment was investigated from
233 Dinniman et al. (2020) model output. The model used is a Regional Ocean Modelling System
234 (ROMS) model, with a 5 km horizontal resolution and 32 terrain following vertical layers and
235 includes sea-ice dynamics, as well as mechanical and thermodynamic interaction between ice
236 shelves and the ocean. The model time run spans seven years and simulates fourteen different
237 tracers to understand dFe supply across the entire Antarctic coastal zone, with the last two years
238 simulating biological uptake. For the purpose of this study, we only use four different dFe
239 sources/tracers in the ASE: ice shelf melt, CDW, sediments and sea ice. Each tracer estimation is
240 independent from each other, meaning that one source does not affect the other, and they have
241 the same probability for biological uptake by phytoplankton. That is, dFe from all sources can
242 equally be taken up by phytoplankton. This is parametrized in the model as all iron molecules
243 being bound to a ligand and therefore remaining in solution in a bioavailable form (Gledhill &
244 Buck, 2012). For a detailed and complete explanation of the model, see Dinniman et al. (2020).

245

246 2.5 Other environmental parameters

247

248 We used SIC data spanning June 1998 to June 2017 from the National Snow and Ice Data Center
249 (Cavalieri et al., 1996). The data are Nimbus-7 SMMR and SSMI/SSMIS passive microwave
250 daily SIC with 25 km spatial resolution. We computed the sea-ice retreat time (IRT) and open
251 water period (OWP) metrics using a 15% threshold (Stammerjohn et al., 2008). Daily data were
252 monthly averaged to perform a spatial correlation analysis (see section 2.6).

253

254 We collected monthly level-4 Optimum Interpolation Sea Surface Temperature (OISST.v2)
255 0.25° high resolution dataset from the National Oceanic and Atmospheric Administration
256 (Huang et al., 2021). Using this dataset compared to others has been proven to be the most
257 suitable for our region of interest (Yu et al., 2023).

258

259 We obtained monthly Photosynthetically Available Radiation (PAR) from the same Globcolour
260 project at the same spatial and temporal resolution (0.04° and 8 days) as chla.

261

262 We used monthly averaged ERA5 reanalysis of zonal (u) and meridional (v) surface wind speed
263 at 10 m above the surface (Hersbach et al., 2020).

264

265 We investigated monthly mean MLD from the Estimating the Circulation and Climate of the
266 Ocean (ECCO) ocean and sea-ice state estimate project (ECCO consortium et al., 2021). The
267 dataset is the version 4, release 4, at 0.5° spatial resolution.

268

269 Variability in the sea-ice landscape can be influenced by the Amundsen Sea Low (ASL) in West
270 Antarctica (Hosking et al., 2013; Turner et al., 2016). We therefore finally looked at the impact
271 of the ASL and its potential influence on sea-ice variability. Monthly ASL indices (latitude,
272 longitude, central and sector pressure) derived from ERA5 reanalysis data were obtained from
273 the ASL climate index page (Hosking et al., 2016).

274

275

276 2.6 Statistical analysis

277

278 Because some of our data were not normally distributed, we consistently applied nonparametric
279 tests throughout our statistical analysis. A Mann-Kendall test was performed to detect linear
280 trends in chla and NPP. A two-tailed non-parametric Spearman correlation metric (rho, *p*) was
281 calculated to investigate the relationship between chla, NPP, and environmental factors, as well
282 as between the phytoplankton bloom and sea-ice phenology metrics. A two-tailed Mann-Whitney
283 test was performed to detect any significant mean differences for chla, sea-ice phenology
284 metrics, MLD, PAR and dFe sources between the two polynyas. Monthly spatial correlations
285 were tested between SIC, winds, chla, NPP, SST, and PAR after removing the seasonality for
286 each parameter. As well, a yearly spatial correlation between chla, NPP and TVFall was
287 performed. The relationships between chla, NPP and environmental factors were explored using
288 a Principal Component Analysis (PCA). No pre-treatment (mean-centering or normalization)
289 was applied to the variables prior to PCA, as all variables are expressed in comparable units and
290 ranges, consistent with common practice in marine biogeochemistry studies (Marchese et al.,
291 2017; Liniger et al., 2020). The Spearman, Mann-Whitney and PCA analysis were conducted
292 using the mean TVFs, MLD, SST, and PAR calculated over the October-March period for each
293 year, with the associated bloom and sea-ice phenology metrics. Every statistical test was run with
294 a 95% (*p*-value < 0.05) confidence level. Our study spans 1998-2017. We are constrained by the
295 start of satellite ocean color data (1998) and the end of the ice shelf basal melt rate record (2017)
296 from Paolo et al (2023).

297

298 **3. Results**

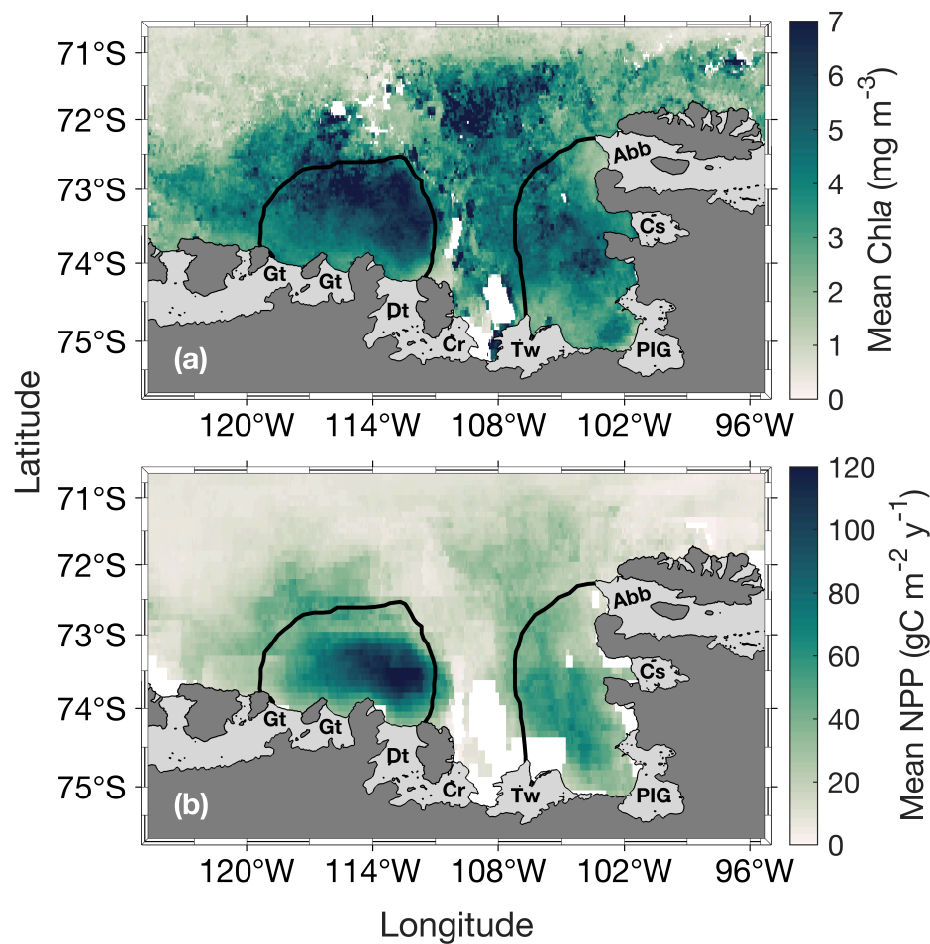
299

300 3.1 Glacial meltwater, chla, and NPP variability

301

302 The annual climatology maps reveal substantially higher chla and NPP in the ASP compared to
303 the PIP (Fig. 2). Chla starts increasing in mid-November to reach its average peak earlier in the
304 PIP than the ASP. At its peak, chla in the ASP is 6.49 mg m^{-3} and 4.94 mg m^{-3} in the PIP (Fig.
305 3a). During the bloom period, chla is also higher in the ASP on average compared to the PIP
306 ($\text{ASP} = 5.21 \pm 1.29 \text{ mg m}^{-3}$; $\text{PIP} = 3.69 \pm 1.11 \text{ mg m}^{-3}$; *p*-value < 0.01; Fig. 3b; Supplementary

307 Table T1). When looking at polynya area integrated values (concentration multiplied by area
 308 gives units of mg m^{-1}), chla is significantly higher in the ASP than in the PIP, and increases with
 309 the polynya area (Supplementary Figs. S1 and S2). NPP is also significantly higher in the ASP
 310 than in the PIP ($1.88 \pm 1.12 \text{ TgC y}^{-1}$ vs $0.85 \pm 0.86 \text{ TgC y}^{-1}$, p-value = 0.004; Supplementary
 311 Fig. S3). No significant interannual trends in mean chla and NPP during the bloom are observed
 312 for either polynya (p-value > 0.1; Fig. 3b; Supplementary Fig. S3). The climatological winter
 313 MLD in the ASP is deeper (MLD ASP = $45.8 \pm 8.0\text{m}$; MLD PIP = $36.4 \pm 7.3\text{m}$; p-value < 0.01;
 314 Fig. 1b), indicating that it may better entrain deeper sources of nutrients into the upper waters for
 315 the following phytoplankton growing season, resulting in higher productivity (Fig. 2).

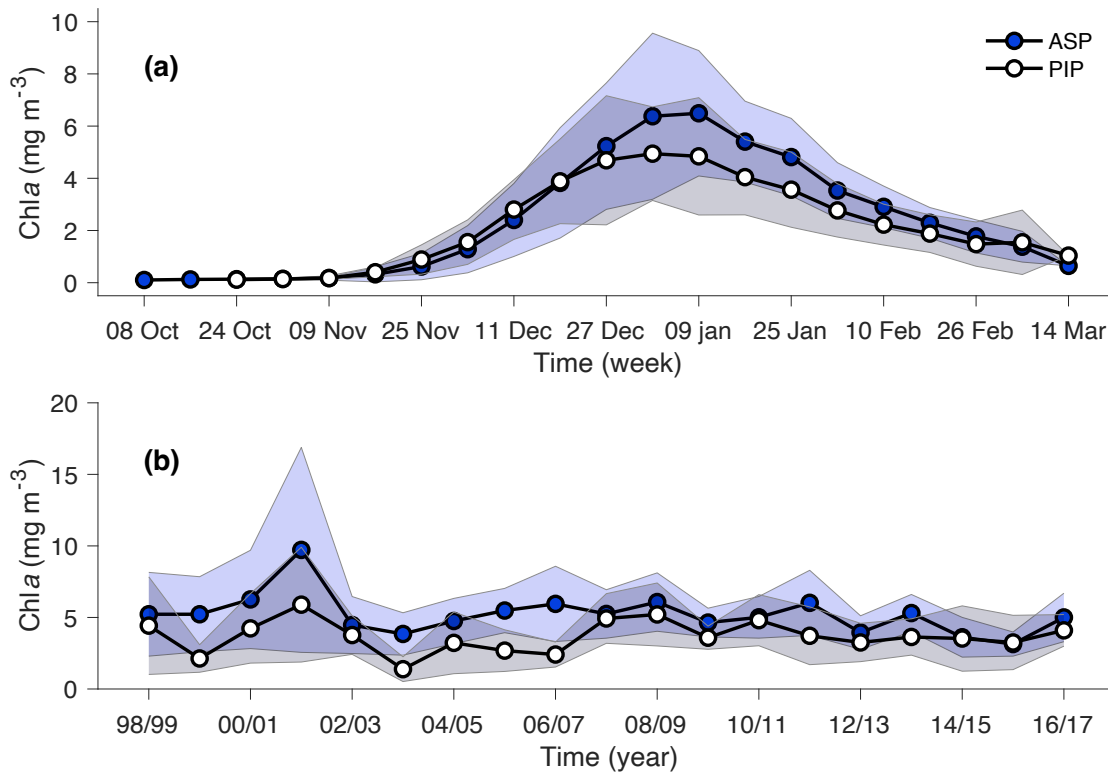


335 **Fig. 2.** Spatial distribution of (a) mean surface chlorophyll-*a* (chla) concentration during the
 336 bloom and (b) net primary productivity (NPP) climatology (1998 – 2017) for the Amundsen

337 (ASP; left) and Pine Island (PIP; right) polynyas. The black lines represent the climatological
338 summer polynyas' boundaries.

339

340



355
356 **Fig. 3.** (a) Weekly chlorophyll-*a* (chl_a) concentration climatology (1998-2017) for the
357 Amundsen (ASP; blue circles) and Pine Island (PIP; white circles) polynyas. (b) Bloom mean
358 chl_a time series of ASP (blue circles) and PIP (white circles). Shaded areas represent the
359 standard deviation for a given year. The relationship between chl_a (in mg m⁻³ and mg m⁻¹) and the
360 polynya size is shown in Supplementary Fig. S2.

361

362 The variability in TVFall is statistically uncorrelated with surface chl_a and NPP in both polynyas
363 from 1998 to 2017 (Fig. 4; Supplementary Fig. S4). However, the relationship becomes strongly
364 significant in the ASP for both mean and maximum chl_a when we remove the chl_a outlier in
365 2001/02 (red data point; Figs. 4a-b), although not for NPP (Supplementary Figs. S4a-b). The
366 positive relationship implies that surface chl_a in the ASP is higher when more glacial meltwater

367 is delivered to the embayment. No strong relationships are observed in the PIP between TVFall,
 368 surface chla and NPP (Figs. 4c-d; Supplementary Figs. S4c-d).

369

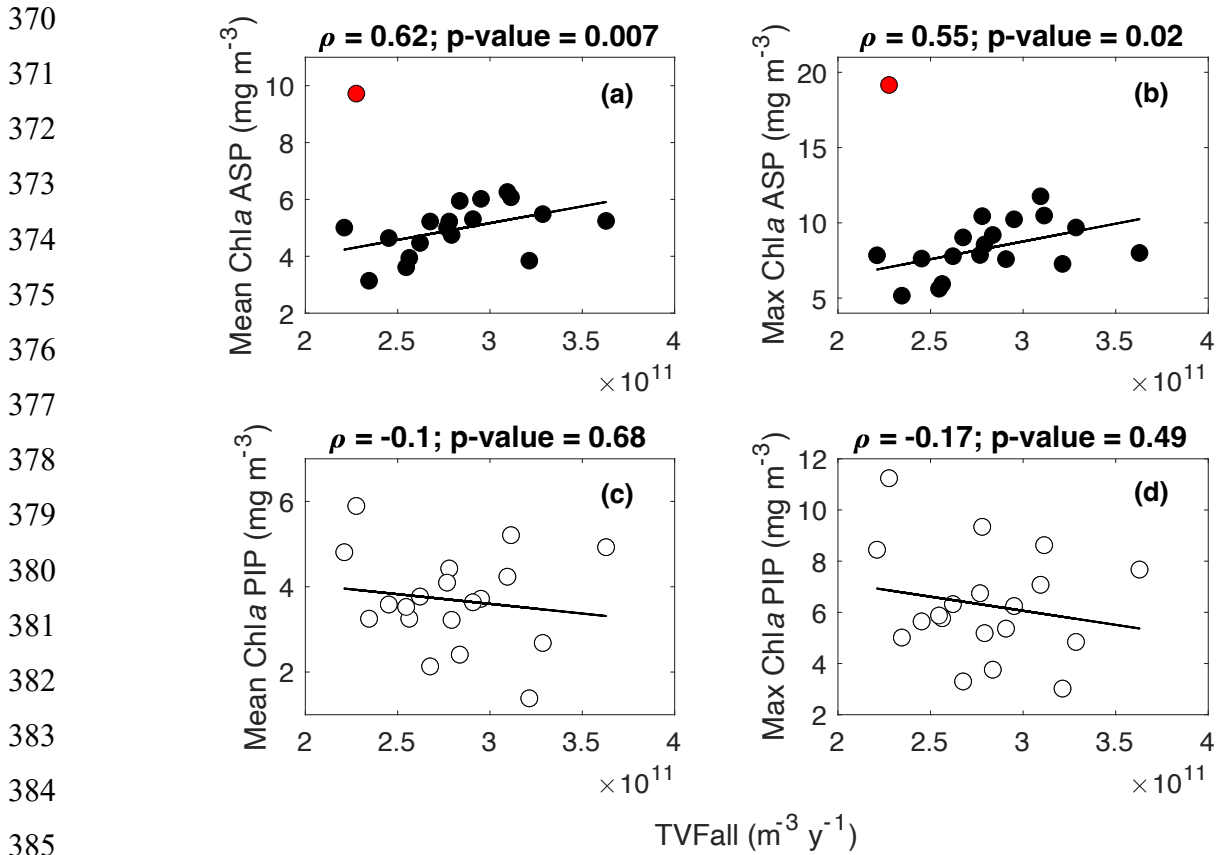


Fig. 4. Scatter plots of mean and maximum (max) surface chlorophyll-*a* (chla) concentrations with the total volume flux (TVFall) for (a-b) the Amundsen (ASP) and (c-d) the Pine Island (PIP) polynyas from 1998 to 2017 ($n=19$). The fitted lines and statistics exclude year 2001/02 (red outlier) for the ASP regressions. If all data is considered, the relationships between mean chla, max chla and TVFall in the ASP are not significant. TVFall is an annual integral representing the sum of all ice shelves (see methods section) for the Amundsen Sea Embayment (ASE).

When fluxes from individual glaciers are considered, PIP chla does not correlate with Abbot, Cosgrove, PIG, Thwaites or TVFpip fluxes (Table 1). On the other hand, ASP chla shows strong relationships with TVFasp, the Dotson and Crosson ice shelves (Table 1), and all ice shelves

398 become significantly correlated with mean and maximum chla when year 2001/02 is removed.
399 There are no statistically significant relationships between individual ice shelves and NPP in
400 either polynyas.

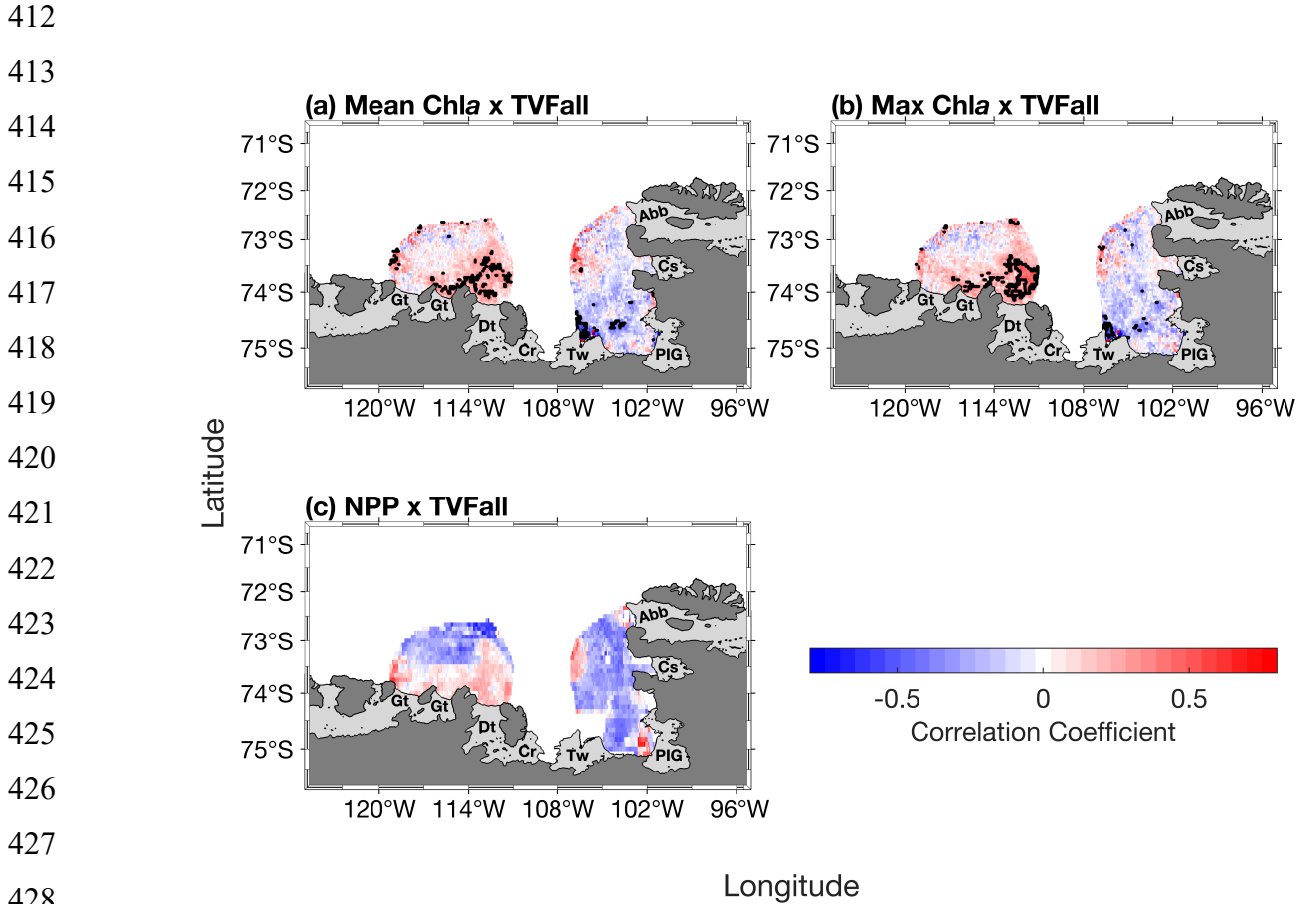
401
402 **Table 1.** Statistical summary (Spearman's rank correlation) of the relationships between ice
403 shelves volume flux, mean and maximum (max) surface chlorophyll-*a* (chla) concentrations
404 (n=19) in both polynyas. The * marks a significant (p-value < 0.05) relationship. All relationships
405 between mean chla, maximum chla and ASP ice shelves become significant when year 2001/02 is
406 removed.

407

408

| | Amundsen Sea polynya (ASP) | | | | Pine Island polynya (PIP) | | | |
|----------|-------------------------------|--------------|-------------|--------------|------------------------------|---------|----------|---------|
| | Mean chla | | Max chla | | Mean chla | | Max chla | |
| | rho | p-value | rho | p-value | rho | p-value | rho | p-value |
| Abbot | / | / | / | / | 0.09 | 0.73 | -0.04 | 0.88 |
| Cosgrove | / | / | / | / | -0.32 | 0.18 | -0.46 | 0.05 |
| PIG | / | / | / | / | -0.04 | 0.88 | -0.13 | 0.61 |
| Thwaites | 0.16 | 0.52 | 0.11 | 0.66 | 0.12 | 0.63 | 0.09 | 0.71 |
| Crosson | 0.43 | 0.07 | 0.50 | 0.03* | / | / | / | / |
| Dotson | 0.48 | 0.04* | 0.54 | 0.02* | / | / | / | / |
| Getz | 0.37 | 0.12 | 0.43 | 0.07 | / | / | / | / |
| TVFasp | 0.42 | 0.07 | 0.46 | 0.05* | / | / | / | / |
| TVFpip | / | / | / | / | 0.009 | 0.97 | -0.1 | 0.68 |

409 Spatially, the mean and maximum chla are strongly correlated with TVFall in southern-eastern
 410 part of the ASP, in front of the Dotson ice shelf (Figs. 5a-b), where a positive relationship with
 411 NPP is also observed (Fig. 5c), although not significant.

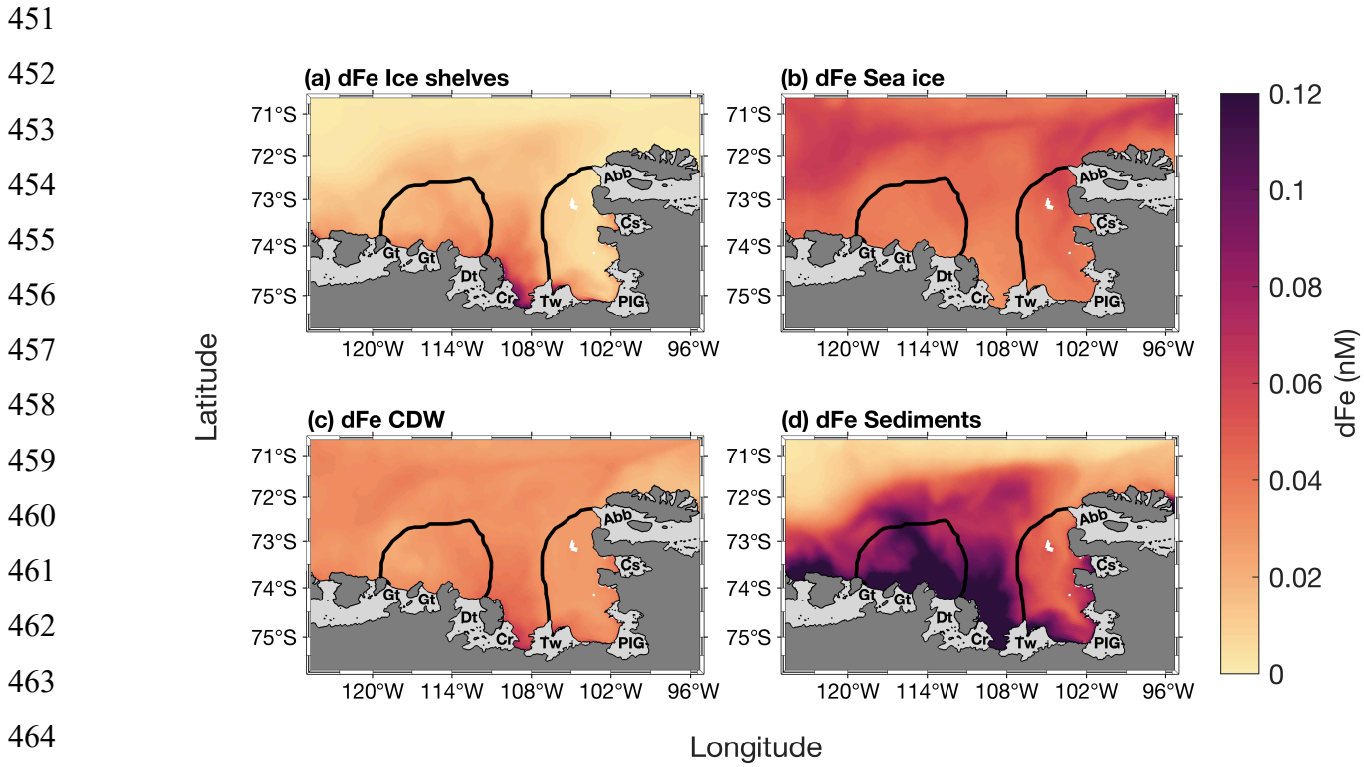


430 **Fig. 5.** Spatial correlation maps between total volume flux (TVFall) and (a) surface mean
 431 chlorophyll-*a* (chla) concentration, (b) surface maximum (max) chla concentration and (c) net
 432 primary productivity (NPP) (n=19). The black contour represents significant correlations at 95%
 433 confidence level. Data outside of the summer climatological polynyas' boundaries were masked
 434 out.

435 3.2 Simulated dFe sources distribution

436 The modelled spatial distribution of surface dFe sources is presented in Fig. 6. On average, the
 437 smallest dFe source in the embayment is from the ice shelves, with a maximum concentration

440 between the Thwaites and Dotson ice shelves. The dFe from sea ice is slightly higher than from
 441 ice shelves and similar over the two polynyas, and is higher near the sea-ice margin (Fig. 6b). The
 442 dFe from CDW is also higher between the Thwaites and Dotson (Fig. 6c). Sediment is the
 443 dominant dFe source (Fig. 6d). Its distribution spreads from 108°W to the western part of the Getz
 444 ice shelf. The highest sediment-sourced dFe concentration is found along the coast and inside the
 445 ASP. On polynya-wide average basis, the sediment reservoir contributes significantly more to total
 446 dFe in the ASP (58.3%, 0.13nM) compared to sea ice (16.5%, 0.04nM), CDW (13.5%, 0.03nM)
 447 and ice shelves (11.7%, 0.03nM). In the PIP, the contribution of sediments is still significantly
 448 higher (41.2%; 0.08nM) but lower than the ASP and the contribution gap with the other sources
 449 decreases. The CDW and sea ice contribute 22.5% (0.04nM) and 18.9% (0.035nM) to the dFe pool
 450 respectively, while ice shelves are still the smallest sources at 14.5% (0.03nM) in the PIP.



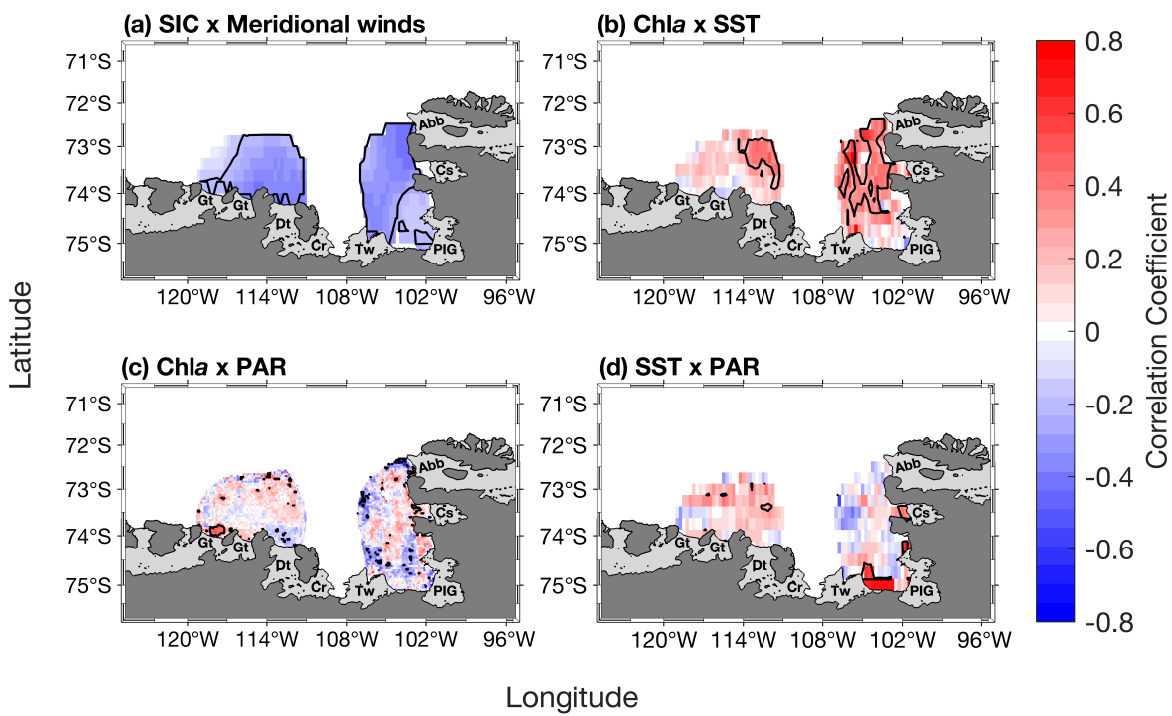
466 **Fig. 6.** Two-years top-100m averaged spatial distribution of surface dissolved iron (dFe)
 467 contribution from (a) ice shelves, (b) sea ice, (c) circum-polar deep water (CDW) and (d) sediments
 468 simulated by the model from Dinniman et al. (2020). The black lines represent the climatological
 469 summer polynyas' boundaries.

471 3.3 Environmental parameters, chla and NPP variability

472

473 During the phytoplankton growth season (October-March), SIC is spatially significantly
 474 anticorrelated to the meridional winds speed in both polynyas (Fig. 7a). Chla is significantly
 475 positively correlated with SST in the eastern ASP, and the whole PIP (Fig. 7b), but weakly with
 476 PAR in both polynyas (Fig. 7c). Finally, PAR and SST are positively related in both central
 477 polynyas, albeit not significantly (Fig. 7d). We note that similar spatial relationships are
 478 observed when NPP is correlated with SST and PAR (Supplementary Fig. S5).

479



494 **Fig. 7.** Spatial correlation map between sea-ice concentration (SIC) and (a) meridional winds.
 495 Spatial correlation maps between mean chlorophyll-*a* (chla) concentration and (b) sea surface
 496 temperature (SST), (c) photosynthetically available radiation (PAR). (d) Spatial correlation map
 497 between PAR and SST. Data span 1998 – 2017 from October to March (n=114). The black contour
 498 represents significant correlations at 95% confidence level. Seasonality was removed before
 499 performing the correlation. Data outside of the summer climatological polynyas' boundaries were
 500 masked out.

502 Regarding the phenology, the bloom start is positively correlated to IRT and negatively with
 503 OWP in the ASP, although not significantly with the OWP (Table 2). This means that the bloom
 504 starts earlier and later as IRT does, and that longer OWP and earlier bloom starts are correlated
 505 with earlier ice retreat. The bloom mean and bloom maximum (max) chla are not correlated with
 506 either IRT and OWP in the ASP. IRT and OWP are significantly related ($p = -0.93$; p-value <
 507 0.001). When year 2001/02 is removed, no significant changes in the relationships between all
 508 parameters are detected. In the PIP, all metrics are significantly related to each other, except for
 509 PAR and OWP (Table 2). That is, the bloom start is positively correlated with IRT and
 510 negatively with OWP, while the bloom duration, mean chla, max chla and NPP are negatively
 511 linked to the IRT and positively with OWP. SST and PAR are negatively correlated with IRT,
 512 and positively with SST. IRT and OWP are significantly related in the PIP ($p = -0.88$; p-value <
 513 0.001).

514

515 **Table 2.** Statistical summary (Spearman's rank correlation) of the relationships between the sea-
 516 ice phenology metrics and environmental parameters (n=19) in both polynyas. The * marks a
 517 significant (p-value < 0.05) relationship. IRT = ice retreat time, OWP = open water period, NPP =
 518 net primary productivity, SST = sea surface temperature, PAR = photosynthetically available
 519 radiation. Removing year 2001/02 for the ASP slightly changes the strength of the relationships
 520 between parameters (i.e., rho) but not the significance.

521

| | Amundsen Sea polynya (ASP) | | | | Pine Island polynya (PIP) | | | |
|----------------|-------------------------------|--------------|-------|---------|------------------------------|---------------|--------------|--------------|
| | IRT | | OWP | | IRT | | OWP | |
| | rho | p-value | rho | p-value | rho | p-value | rho | p-value |
| Bloom start | 0.51 | 0.03* | -0.43 | 0.07 | 0.56 | 0.02* | -0.48 | 0.04* |
| Bloom duration | -0.12 | 0.63 | 0.09 | 0.71 | -0.56 | 0.02* | 0.59 | 0.01* |
| Bloom mean | 0.19 | 0.44 | -0.33 | 0.17 | -0.67 | 0.003* | 0.50 | 0.04* |
| Bloom max | 0.24 | 0.32 | -0.35 | 0.14 | -0.65 | 0.005* | 0.52 | 0.03* |
| NPP | -0.55 | 0.02* | 0.45 | 0.05 | -0.72 | 0.001* | 0.54 | 0.02* |

| | | | | | | | | | |
|-----|-----|-------|------|-------|------|--------------|---------------|-------------|--------------|
| 522 | SST | -0.09 | 0.72 | -0.01 | 0.96 | -0.57 | 0.02* | 0.52 | 0.03* |
| 523 | PAR | -0.09 | 0.72 | 0.05 | 0.84 | -0.62 | 0.007* | 0.38 | 0.12 |

525

526 We explore the relationships between phytoplankton bloom phenology metrics and their
 527 potential environmental drivers by conducting a multivariate PCA for both polynyas (Fig. 8).
 528 The PCA reduces our datasets (11 variables) and breaks them down into dimensions that capture
 529 most of the variability and relationships between all variables. Arrows indicate the contribution
 530 of each variable to the dimensions, with longer arrows representing stronger influence.
 531 Observations (in our case, years) positioned in the direction of an arrow are more influenced by
 532 that variable. In the ASP (Fig. 8a), the first two principal components explain 55.3% of the total
 533 variance (Dim1: 35%, Dim2: 20.3%). NPP in the ASP is closely associated with BD, indicating
 534 that the bloom duration is the primary driver of production. On the other hand, environmental
 535 vectors such as TVFall and TVFasp project more strongly onto Dim2 with the bloom mean chla,
 536 indicating that meltwater input may influence surface chla interannual variability, and is less
 537 directly tied to NPP. We note that when year 2001/02 is removed, the relationship between
 538 TVFasp and TVFall becomes much stronger with BM (Supplementary Fig. S6a) and is slightly
 539 anticorrelated to SST and MLD. In the PIP (Fig. 8b), the first two components account for 63.7%
 540 of the total variance (Dim1: 46.7%, Dim2: 17%). Compared to the ASP, both NPP and BM
 541 cluster strongly with BD and PAR on Dim1. Additionally, IRT, OWP and SST and MLD aligned
 542 along Dim1, which explains 46.7% of the total variance compared to 35% for the ASP,
 543 suggesting that physical conditions might play a stronger structuring role in PIP compared to the
 544 ASP. In contrast, TVFall and TVFpip stand alone and align more strongly with Dim2, suggesting
 545 a less dominant influence of meltwater on BM and NPP variability in the PIP. The summer
 546 polynya-averaged PAR and MLD are significantly stronger and deeper, respectively, in the ASP
 547 compared to the PIP during the bloom season (MLD ASP = 28.5 ± 5.7 m; MLD PIP = $24.9 \pm$
 548 3.7 m; p-value = 0.03 and PAR ASP = 31.5 ± 5.4 Einstein $m^{-2} d^{-1}$; PAR PIP = 26.5 ± 6.7 Einstein
 549 $m^{-2} d^{-1}$; p-value = 0.02).

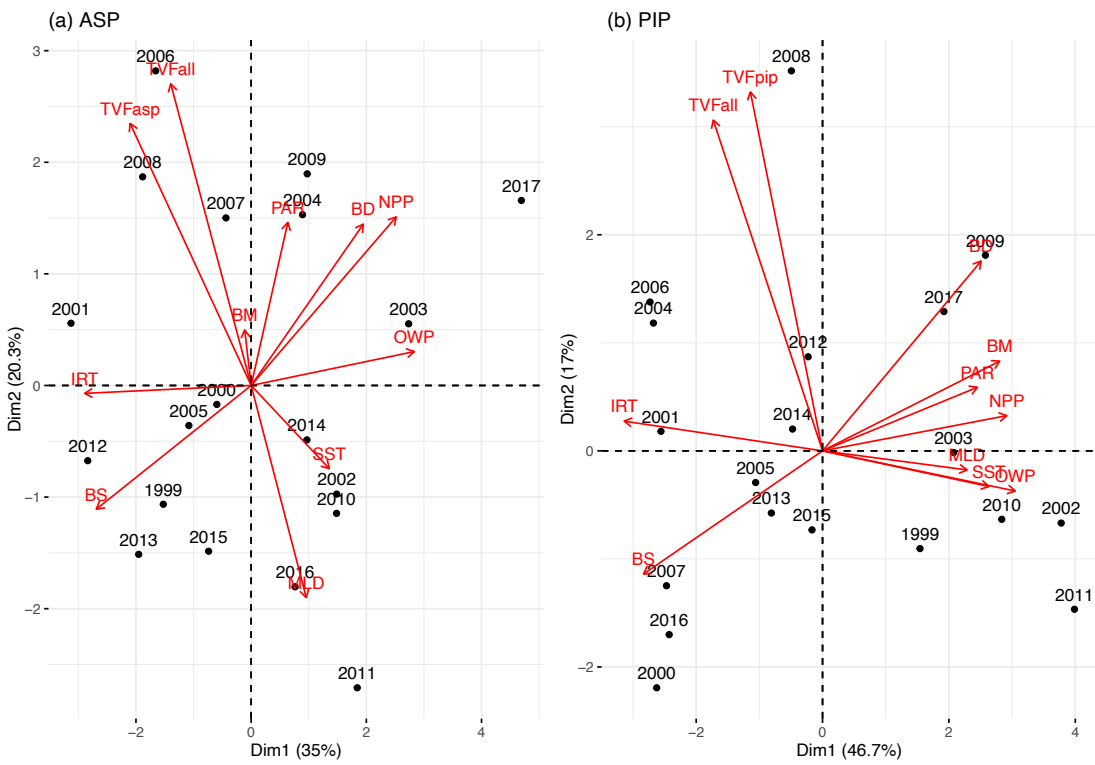


Fig. 8. Principal component analysis biplot of environmental parameters (red) and years (black) for (a) the Amundsen (ASP) and (b) the Pine Island (PIP) polynyas. TVFasp = total volume flux for ASP; TVFpip = total volume flux for PIP; TVFall = total volume flux for all ice shelves; BM = bloom mean; PAR = photosynthetically available radiation; BD = bloom duration; NPP = net primary productivity; OWP = open water period; SST = sea surface temperature; MLD = mixed-layer depth; BS = bloom start; IRT = ice retreat time. The same plot is presented in supplementary Fig. S6, but removing year 2001/02 for the ASP, emphasizing the relationship between total volume flux (TVFall, TVFasp) and BM in the ASP.

Finally, we find on average weak spatial negative relationships between SIC and ASL latitude, longitude, mean sector and actual central pressure in both polynyas during the growing season (Supplementary Fig. S7), and only slightly significant in the eastern PIP.

581 **4. Discussion**

582

583 **4.1 Effect of glacial meltwater on phytoplankton chla and NPP**

584

585 The relationship between glacial meltwater, surface chla and NPP observed over the last two
586 decades was distinctly different between the two polynyas. In the ASP, we found that enhanced
587 glacial meltwater translates into higher surface chla, but not with NPP (when removing year
588 2001/02; Figs. 4a-b; Supplementary Fig. S6a). Modelling results (Fig. 6) suggest that sediment
589 from the seafloor is the main source of dFe in the ASP, but this source is also linked to glacial
590 melt. Ice shelf glacial meltwater drives the meltwater pump, which brings up mCDW and fine-
591 grained subglacial sediments to the surface. This result is in agreement with previous research:
592 Melt-laden modified CDW flowing offshore from the Dotson ice shelf to the central ASP
593 (Sherrell et al., 2015), and resuspended sediments (Dinniman et al., 2020; St-Laurent et al., 2017;
594 2019) have been identified as significant sources of dFe to be used by phytoplankton.
595 Interestingly, both dFe supplied from ice shelves and CDW are most important in front of the
596 Thwaites and Crosson ice shelves, where the area averaged basal melt rate, and thus likely the
597 area averaged meltwater pumping (Jourdain et al., 2017), are typically strongest in observations
598 (Adusumilli et al., 2020; Rignot et al., 2013) and modelling (Fig. 6). The year 2001/02 does not
599 stand out as being influenced by any specific parameter in the ASP compared to other years (Fig.
600 8a, Supplementary Fig. S6a). The anomalously high surface chla observed during this year, as
601 also reported by Arrigo et al. (2012), may result from exceptional conditions that were not
602 captured by the parameters analysed in our study, for instance, an imbalance in the grazing
603 pressure. Interestingly, surface chla and NPP exhibit contrasting trends when averaged across the
604 polynya. While TVFall may explain some of the variance in surface chla, it does not account for
605 the variance in NPP, whether assessed through direct or multivariate relationships. This
606 decoupling between chla and NPP in the ASP suggests that glacial meltwater, while enhancing
607 surface phytoplankton biomass through nutrient delivery, may also promote vertical mixing. This
608 mixing deepens the mixed layer, reducing light availability and constraining photosynthetic
609 rates. These rates are influenced by fluctuations in the MLD, even in the presence of high
610 biomass and sufficient macronutrients. The summer MLD is deeper in the ASP, which would
611 decrease light availability, despite higher PAR compared to the PIP. Previous studies report that

612 the small prymnesiophyte *P. antarctica*, a low-efficiency primary producer (Lee et al., 2017), is
613 better adapted to deeper mixed layers and therefore lower light conditions (Alderkamp et al.,
614 2012; Mills et al., 2010) and could contribute to high surface chla decoupled from NPP, as
615 observed in the ASP. This is consistent with past *in situ* studies showing systematic differences
616 in mixed-layer structure between the two polynyas. The PIP commonly exhibits a shallow,
617 strongly stratified surface mixed layer while the ASP is more variable and has been observed to
618 host deeper MLD (Alderkamp et al., 2012; Park et al., 2017; Yager et al., 2016; Mills et al.,
619 2012). Near glacier and ice-shelf fronts, entrainment of iron-rich deep waters rising to the surface
620 through the meltwater pump can also produce surface chla maxima (high biomass from. *P.*
621 *antarctica*) without proportional increases in depth-integrated productivity due to self-shading
622 (Twelves et al., 2021). Further from the coast, meltwater spreading at neutral buoyancy
623 strengthens stratification, limiting vertical nutrient fluxes and thereby suppressing NPP despite
624 elevated chla. These dual mechanisms are consistent with observational and modelling studies of
625 meltwater entrainment and dispersal (Randall-Goodwin et al., 2015; St-Laurent et al., 2017;
626 Dinniman et al., 2020; Forsch et al. 2021), and suggest that spatial heterogeneity in plume
627 dynamics could explain the observed chla and NPP mismatch.

628
629 In the PIP, we did not find any long-term relationships between the phytoplankton bloom, NPP
630 and glacial meltwater. Variability in ice shelf glacial meltwater may not have the same effect on
631 the surface chla and NPP in the PIP compared to the ASP. Iron delivered from glacial melt
632 process related in the PIP and west of it could accumulate and follow the westward coastal
633 current, towards the ASP (St-Laurent et al., 2017). These sources would include dFe from
634 meltwater pumped CDW, sediments and ice shelves, all of which are higher in front of the
635 Crosson ice shelf, west of the PIP (Fig. 6). With the coastal circulation, this would make dFe
636 supplied by glacial meltwater greater in the ASP, thereby contributing to the higher productivity
637 in the ASP. Recently, subglacial discharge (SGD) was shown to have a different impact on basal
638 melt rate in the ASE polynyas (Goldberg et al., 2023), where PIG had a lot less relative increase
639 in melt with SGD input than Thwaites or Dotson/Crosson. Thus, assuming a direct relationship
640 between meltrate, SGD and dFe sources, the signal in the PIP (fed by PIG melt) will be much
641 weaker than in the ASP (fed by upstream Thwaites, Crosson and local Dotson due to the
642 circulation), which might also explain the discrepancies between the PIP and ASP. A stronger

643 meltwater-driven stratification may also dominate in the PIP, reducing vertical nutrient
644 replenishment and thereby limiting biomass growth (Oh et al., 2022), even where TVFall is high,
645 hence leading to a direct negative relationship observed compared to the ASP (Fig. 4;
646 Supplementary Fig. S4). The model outputs used here are critical to understand the spatial
647 distribution of dFe in the embayment. They strongly suggest, but do not definitively demonstrate,
648 the role of dFe in influencing the phytoplankton bloom interannual variability.

649

650 Satellite algorithms commonly estimate NPP from surface chla, but the approach and
651 assumptions vary across models. The VGPM relates chla to depth-integrated photosynthesis
652 through empirical relationships with light and temperature (Behrenfeld & Falkowski, 1997). In
653 contrast, the Carbon-based Productivity Model (CbPM) emphasizes phytoplankton carbon
654 biomass and growth rates derived from satellite optical properties, decoupling productivity
655 estimates from chla alone (Westberry et al., 2008). The CAFE model (Carbon, Absorption, and
656 Fluorescence Euphotic-resolving model) integrates additional physiological parameters such as
657 chla fluorescence and absorption to better constrain phytoplankton carbon fixation (Silsbe et al.,
658 2016). In the Southern Ocean, where light limitation, iron supply, and community composition
659 strongly influence the relationship between chla and productivity, these algorithmic differences
660 can yield substantial variability in NPP estimates (Ryan-Keogh et al., 2023), with studies
661 showing that VGPM-type models often outperform CbPM in coastal Southern Ocean regions
662 (Jena et al., 2020). Because the VGPM algorithm does not explicitly incorporate the MLD, but
663 instead estimates primary production integrated over the euphotic zone based on surface chla,
664 PAR, and temperature, it may not fully capture the influence of variable MLD or subsurface
665 processes related to glacial melt, which could contribute to the observed decoupling between
666 chla and NPP. Therefore, while the observed decoupling between chla and NPP in the ASP
667 might also come from our choice of dataset, the VGPM model may be more appropriate for
668 coastal polynya environments, such as those in the Amundsen Sea. We finally note as a
669 limitation that satellite-derived chla and VGPM NPP estimates lack the vertical resolution
670 needed to resolve sub-plume stratification and mixing processes (e.g., fine-scale vertical
671 gradients in iron or nutrient fluxes), so our mechanistic interpretations of surface chla vs. depth-
672 integrated productivity decoupling must be taken with caution.

673

674 Direct observations from Sherrell et al. (2015) showed higher chla in the central ASP while
675 surface dFe was low weeks before the bloom peak. This suggests a continuous supply and
676 consumption of dFe in the area, most likely from the circulation, as mentioned earlier.
677 Considering the long residence time of water masses in both polynyas (about 2 years (Tamsitt et
678 al., 2021)), and the daily dFe uptake by phytoplankton ($3\text{-}196 \text{ pmol l}^{-1} \text{ d}^{-1}$ (Lannuzel et al.,
679 2023)), we also hypothesise that any dFe reaching the upper ocean from external sources is
680 quickly used and unlikely to remain readily available for phytoplankton in the following spring
681 season.

682

683 In recent model simulations with the meltwater pump turned off, Fe becomes the principal factor
684 limiting phytoplankton growth in the ASP (Oliver et al., 2019). However, the transport of Fe-rich
685 glacial meltwater outside the ice shelf cavities and to the ocean surface depends strongly on the
686 local hydrography. While Naveira Garabato et al. (2017) suggested that the glacial meltwater
687 concentration and settling depth (neutral buoyancy) outside the ice shelf cavities is controlled by
688 an overturning circulation driven by instability, others suggest that the strong stratification plays
689 an important role in how close to the surface the buoyant plume of said meltwater can rise
690 (Arnscheidt et al., 2021; Zheng et al., 2021). Therefore, high melting years and greater TVFall
691 might not necessarily translate into a more iron-enriched meltwater delivered to the surface
692 outside the ice shelf cavities, close to the ice shelf edge, as rising water masses may be either
693 prevented from doing so, or be transported further offshore in the polynyas where the
694 phytoplankton bloom occurs, before they can resurface (Herraiz-Borreguero et al., 2016).

695

696 Although several Fe sources can fuel polynya blooms, and they depend on processes mentioned
697 above, Fe-binding ligands may ultimately set the limit on how much of this dFe stays dissolved
698 in the surface waters (Gledhill and Buck, 2012; Hassler et al., 2019; Tagliabue et al., 2019).
699 Models of the Amundsen Sea (Dinniman et al., 2020, 2023; St-Laurent et al., 2017, 2019) did not
700 include Fe complexation with ligands and assumed a continuous supply of available dFe for
701 phytoplankton. Spatial and seasonal data on Fe-binding ligands along the Antarctic coast remain
702 extremely scarce and their dynamics are poorly understood (see Smith et al. (2022) for a
703 database of publicly available Fe-binding ligand surveys performed south of 50°S). Field
704 observations in the ASP and PIP suggest that the ligands measured in the upwelling region in

705 front of the ice shelves had little capacity to complex any additional Fe supplied from glacial
706 melt. As a consequence, much of the glacial and sedimentary Fe supply in front of the ice
707 shelves could be lost via particle scavenging and precipitation (Thuróczy et al., 2012). This was
708 also observed by van Manen et al. (2022) in the ASP. However, within the polynya blooms,
709 Thuróczy et al. (2012) found that the ligands produced by biological activity were capable of
710 stabilising additional Fe supplied from glacial melt, where we observed the highest productivity.
711 The production of ligands by phytoplankton would increase the stock of bioavailable dFe and
712 further fuel the phytoplankton bloom in the polynyas, potentially highlighting the dominance
713 of *P. antarctica*, which uses iron-binding ligands more efficiently than diatoms (Thuróczy et al.,
714 2012), even under low light conditions. Model development and sustained field observations on
715 dFe availability, including ligands, are needed to adequately predict how these may impact
716 biological productivity under changing glacial and oceanic conditions, now and in the future.
717

718 Overall, the discrepancies observed between the ASP and PIP point to a complex set of ice-
719 ocean-sediment interactions, where several co-occurring processes and differences in
720 hydrographic properties of the water column influence dFe supply and consequent primary
721 productivity.

722
723 4.2 Possible drivers of the difference in phytoplankton surface chla and NPP between the
724 two polynyas
725

726 The biological productivity is higher in the ASP than the PIP, consistent with previous studies
727 (Arrigo et al., 2012; Park et al., 2017). In section 4.1, we mentioned the suspected underlying
728 hydrographic drivers of these differences. We related the higher biological productivity in the
729 ASP to a potentially greater supply of iron from melt-laden dFe-enriched mCDW and sediment
730 sources, but this difference in productivity could also be attributed to other local features. The
731 Bear Ridge grounded icebergs on the ASP's eastern side (Bett et al., 2020) could add to the
732 overall meltwater pump strength. They can enhance warm CDW intrusions to the ice shelf cavity
733 (Bett et al., 2020), increasing ice shelf melting and subsequent stronger phytoplankton bloom
734 from the meltwater pump activity. These processes are weaker or absent in the PIP. Few sources
735 other than glacial meltwater may influence the bloom in the PIP. For instance, dFe in the

736 euphotic zone can also be sustained by the biological recycling, as shown in the PIP by Gerringa
737 et al. (2020).

738

739 Sea ice could also partly explain the difference in chla magnitudes, NPP, and variability between
740 the ASP and PIP. The strong spatial correlation between SIC and meridional winds (Fig. 7a)
741 indicates that southerly winds can export the coastal sea ice offshore and play a significant role
742 in opening the polynyas. In the ASP compared to the PIP, sea ice retreats earlier (IRT = Jan 1st ±
743 14d vs Jan 18th ± 17d, p-value = 0.003), the open water period is longer (OWP = 61 ± 16d vs 44
744 ± 22d, p-value < 0.001), and the SIC is lower (Supplementary Fig. S8). In the ASP, an early sea-
745 ice retreat leads to an earlier bloom start, but the longer open water period is not significantly
746 associated with greater bloom mean or maximum chla (Table 2). On the other hand in the PIP,
747 an early sea-ice retreat also triggers an early bloom start, but the longer open duration is
748 associated with warmer water, higher bloom mean chla, maximum chla, and NPP. These results
749 suggest that different processes might drive phytoplankton growth variability in the two
750 polynyas. In the ASP, it is likely the replenishment of dFe mentioned above that mostly
751 influences the bloom. In the PIP, higher SIC can delay the retreat time and shorten the open
752 water season (Table 2, Supplementary Fig. S8), leading to lower chla and NPP compared to the
753 ASP. The significant negative relationships between IRT, PAR, chla and NPP in the PIP (Table
754 2, Supplementary Fig. S6) suggests a strong light limitation relief in the polynya. This light
755 limitation hypothesis is further supported by the high correlation between polynya-averaged chla
756 mean with PAR and SST in the PIP across the 19 years of study, compared to the lack of
757 correlation in the ASP (Supplementary Table T2; p-value < 0.01 for all relationships in the PIP).
758 While *P. antarctica* is usually the main phytoplankton species dominating in both polynyas, the
759 combination of light-limitation relief and higher SST may create better conditions for a stratified
760 and warmer environment that would favor diatom (Arrigo et al., 1999; van Leeuwe et al., 2020),
761 as recently observed in the ASP (Lee et al., 2022). The positive association of PAR, SST and
762 chla with MLD likely reflects conditions around sea-ice retreat (all negatively associated with
763 IRT), when enhanced wind mixing deepens the mixed layer and replenishes surface nutrients
764 while light availability and SST increases. This nutrient-light co-limitation phase supports high
765 biomass accumulation, likely from diatoms. Similar results have been reported by Park et al.
766 (2017). They found that the PIP was dFe was not limited by dFe, potentially from biological

767 recycling (Gerringa et al., 2020), compared to an iron-limited ASP. We hypothesise that the
768 connection between glacial meltwater and chla that we found in the ASP is a response to iron
769 input (also observed by Park et al. (2017) during incubation experiments) compared to the PIP,
770 where light and temperature seem to play a more significant role in driving the phytoplankton
771 bloom variability. Hayward et al. (2025) showed a decline in diatoms from 1997 to 2017 in the
772 PIP. However, they observed an increase in diatoms after 2017, linked to regime shift in sea ice.
773 Their study also indicates that diatoms are competitively disadvantaged under iron-depleted
774 conditions. *P. antarctica*, which relies on dFe supplied by ocean circulation, would then tend to
775 dominate in the ASP. Such shifts in phytoplankton composition are likely to affect carbon
776 export, grazing, and higher trophic levels. Additional long-term data on inter-annual variability
777 in phytoplankton composition and physiology will be essential to fully understand these
778 relationships.

779

780 Finally, the weak relationships between the ASL indices and SIC might be owing to the seasonal
781 variation of the ASL, where its position largely varies during summer, and its impact in shaping
782 coastal sea ice is also greater during winter and autumn in the Amundsen-Bellingshausen region
783 (Hosking et al., 2013). The lack of strong significant relationships overall does not allow us to
784 conclude that the ASL plays an important role in shaping the coastal polynyas landscape and
785 influencing chla variability.

786

787 4.3 Limitations and future directions

788

789 We acknowledge that elevated concentrations of suspended sediments (and non-
790 photosynthetically active particles in general) near the ocean surface can impart optical
791 signatures that bias satellite-derived chla high in coastal waters. Consequently, the higher chla
792 observed in the ASP relative to the PIP, as well as the weak correspondence between chla and
793 NPP in ASP, may reflect some sediment-driven optical effects rather than enhanced
794 phytoplankton biomass or productivity alone. While our results are consistent with known
795 differences in iron supply and mixed-layer dynamics between the two polynyas, the potential
796 contribution of sediment-related bias cannot be ruled out and should be acknowledged when
797 interpreting spatial contrasts in satellite chla on the Antarctic shelf.

798

799 While it seems reasonable that the higher ASP productivity could be driven by more iron
800 delivered through a stronger meltwater pump downstream of the PIP, our data cannot confirm
801 this hypothesis. To accurately understand the role of iron through the meltwater pump process,
802 we would need to quantify the fraction of meltwater and glacial modified water (mix of CDW
803 and ice shelf meltwater) reaching the ocean surface, together with the iron content. Obtaining
804 this information is challenging over the decadal time scales considered and the method used in
805 our study. Here, our intention was to provide valuable insights into the potential drivers of our
806 results, and highlight the benefit of remote sensing, in this poorly observed environment. Our
807 work directly aligns with Pan et al. (2025), who investigated the long-term relationship between
808 sea surface glacial meltwater and satellite surface chla in the Western Antarctic Peninsula, and
809 found a strong relationship between the two parameters, highlighting the importance of glacial
810 meltwater discharge in regions prone to extreme and rapid climate changes.

811

812 In multimodel climate change simulations, Naughten et al (2018) showed an increase of ice
813 shelves melting up to 90% on average, attributed to more warm CDW on the shelf, due to
814 atmospherically driven changes in local sea-ice formation. More recently, Dinniman et al. (2023)
815 also highlighted the impact of projected atmospheric changes on Antarctic ice sheet melt. They
816 showed that strengthening winds, increasing precipitation and warmer atmospheric temperatures
817 will increase heat advection onto the continental shelf, ultimately increasing basal melt rate by
818 83% by 2100. Compared to present climate simulations, their simulation showed a 62% increase
819 in total dFe supply to shelf surface waters, while basal melt driven overturning Fe supply
820 increased by 48%. The ice shelf melt and overturning contributions varied spatially, increasing in
821 the Amundsen-Bellingshausen area and decreasing in East Antarctica. This implies that, under
822 future climate change, phytoplankton productivity could show stronger spatial asymmetry
823 around Antarctica. The increasing melting and thinning of ice shelves will eventually result in
824 more numerous calving events and drifting icebergs (Liu et al., 2015). Model simulations
825 stressed the importance of ice shelves and icebergs in delivering dFe to the SO (Death et al.,
826 2014; Person et al., 2019), increasing offshore productivity. As Fe will likely be replenished and
827 sufficient from increasing melting in coastal areas, it is possible that the system will shift from

828 Fe-limited to being limited by nitrate, silicate, or even manganese (Anugerahanti and Tagliabue,
829 2024), while offshore SO productivity will likely remain Fe-dependent (Oh et al., 2022).

830

831 **5. Conclusions**

832

833 Using spatial and multivariate approaches, our study explored the variability of surface chla and
834 NPP in the Amundsen Sea polynyas over the last two decades, with a focus on the main
835 environmental characteristics of the ASE. We found a strong relationship between ice shelf
836 melting and surface chla in the ASP when year 2001/02 was removed, a result in agreement with
837 the ASPIRE field studies and previous satellite analyses. On the other hand, we did not find clear
838 evidence of such a relationship in the PIP, where light, sea surface temperature and open water
839 availability seem more important. The differences between the polynyas may lie in hydrographic
840 properties, or the use of satellite remote sensing itself, which cannot tell us about processes such
841 as Fe supply, bioavailability and phytoplankton demand. To gain greater insight, we referred to
842 model simulations that showed the spatial variability in the magnitude of iron sources. Our
843 results call for sustained *in situ* observations (e.g., moorings equipped with trace-metal clean
844 samplers, and physical sensors to better understand year-to-year water mass meltwater fraction
845 and properties) to elucidate these long-term relationships. Satellite observations are a powerful
846 tool to investigate the relationship between glacial meltwater and biological productivity on such
847 time scales, which has until now relied almost exclusively on field observations and modelling.
848 Using such tools, we showed how the relationship between phytoplankton and the environment
849 varies spatially and temporally across 19 years.

850

851 **Appendices**

852 No appendices are related to the manuscript.

853

854 **Data availability**

855 Bathymetry data (Amante & Eakins, 2009) was taken from the NOAA website
856 (<http://www.ngdc.noaa.gov/mgg/global/global.html>). Mixed-layer depth (ECCO Consortium et
857 al., 2021) can be accessed here:

858 https://podaac.jpl.nasa.gov/dataset/ECCO_L4_MIXED_LAYER_DEPTH_05DEG_MONTHLY

859 V4R4. Satellite surface chlorophyll-*a* and photosynthetically available radiation were
860 downloaded from <https://www.globcolour.info/>. Sea surface temperature (Huang et al., 2021)
861 can be found here <https://psl.noaa.gov/data/gridded/data.noaa.oisst.v2.highres.html>. Wind re-
862 analysis data (Hersbach et al., 2020) are available at
863 [https://cds.climate.copernicus.eu/datasets/reanalysis-era5-single-levels-monthly-
864 means?tab=download](https://cds.climate.copernicus.eu/datasets/reanalysis-era5-single-levels-monthly-means?tab=download). Sea-ice concentration (Cavalieri et al., 1996) was obtained from
865 <https://nsidc.org/data> and Net Primary productivity (Behrenfeld and Falkowski, 1997) was
866 downloaded from <http://sites.science.oregonstate.edu/ocean.productivity/index.php>. Circumpolar
867 surface model output from Dinniman et al (2020) can be found at [https://www.bco-
868 dmo.org/dataset/782848](https://www.bco-dmo.org/dataset/782848). The Amundsen Sea Low index (Hosking et al., 2016) data are available
869 at http://scotthosking.com/asl_index.

870

871 **Author contributions**

872 GL conceptualised and led the study; MSD provided the dissolved iron model output. All authors
873 were involved in the interpretation of the results, the revision, and the writing of the final version
874 of the paper.

875

876 **Competing interest**

877 We declare having no competing interests.

878

879 **Acknowledgments**

880 We would like to thank the University of Tasmania, the Australian Research Council (ARC)
881 Centre of Excellence for Climate Extremes (CE170100023), and the Australian Centre for
882 Excellence in Antarctic Science (ACEAS; SR200100008) for financial support. Delphine
883 Lannuzel is funded by the ARC through a Future Fellowship (L0026677). Sebastien Moreau
884 received funding from the Research Council of Norway (RCN) for the project “I-CRYME:
885 Impact of CRYosphere Melting on Southern Ocean Ecosystems and biogeochemical cycles”
886 (grant number 335512) and for the Norwegian Centre of Excellence “iC3: Center for ice,
887 Cryosphere, Carbon and Climate” (grant number 332635). Michael Dinniman was supported by
888 the U.S National Science Foundation grant OPP-1643652. We are also grateful to Will Hobbs,
889 Rob Massom and Patricia Yager for their knowledgeable input. We thank Vincent Georges for

890 some preliminary work as part of his masters' internship. We are very grateful to Fernando S.
891 Paolo for his early input and help with the glacial meltwater dataset. We thank the data providers
892 mentioned in the methods section for making their data available and free of charge.

893

894 **Financial support**

895 All financial support were mentioned in the Acknowledgment section.

896

897 **References**

898 Adusumilli, S., Fricker, H. A., Medley, B., Padman, L., and Siegfried, M. R.: Interannual
899 variations in meltwater input to the Southern Ocean from Antarctic ice shelves, *Nat. Geosci.*, 13,
900 616–620, <https://doi.org/10.1038/s41561-020-0616-z>, 2020.

901 Alderkamp, A-C., Mills, M. M., van Dijken, G. L., Lann, P., Thuróczy, C-E., Gerringa, L. J.A.,
902 de Barr, H. J. W., Payne, C. D., Visser, R. J. W., Buma A. G. J., and Arrigo, K. R.: Iron from
903 glaciers fuels phytoplankton blooms in the Amundsen Sea (Southern Ocean): Phytoplankton
904 characteristics and productivity, *Deep-Sea Res. II.*, 71–76, 32–48,
905 <https://doi.org/10.1016/j.dsr2.2012.03.005>, 2012.

906

907 Amante, C., and Eakins, B.W.: ETOPO1 1 Arc-Minute Global Relief Model: Procedures, Data
908 Sources and Analysis, NOAA Technical Memorandum NESDIS NGDC-24. National
909 Geophysical Data Center [data set], NOAA, doi:10.7289/V5C8276M, 2009.

910

911 Anugerahanti, P. and Tagliabue, A.: Response of Southern Ocean Resource Stress in a Changing
912 Climate, *Geophys. Res. Lett.*, 51, e2023GL107870, <https://doi.org/10.1029/2023GL107870>,
913 2024.

914 Ardyna, M., Claustre, H., Sallée, J-B., D'Ovidio, F., Gentili, B., van Dijken, G. L., D'Ortenzio,
915 F., and Arrigo, K. R.: Delineating environmental control of phytoplankton biomass and
916 phenology in the Southern Ocean, *Geophys. Res. Lett.*, 44, 5016–5024, doi:10.1002/
917 2016GL072428, 2017.

918 Ardyna, M., Mundy, C. J., Mayot, N., Matthes, L. C., Oziel, L., Horvat, C., Leu, E., Assmy, P.,
919 Hill, V., Matrai, P. A., Gale, M., Melnikov, I. A., and Arrigo, K. R.: Under-Ice Phytoplankton
920 Blooms: Shedding Light on the “Invisible” Part of Arctic Primary Production, *Front. Mar. Sci.*,
921 7, <https://doi.org/10.3389/fmars.2020.608032>, 2020.

922 Arnscheidt, C. W., Marshall, J., Dutrieux, P., Rye, C. D., and Ramadhan, A.: On the Settling
923 Depth of Meltwater Escaping from beneath Antarctic Ice Shelves, *JPO*, 51, 2257–2270,
924 <https://doi.org/10.1175/JPO-D-20-0286.1>, 2021.

925 Arrigo, K. R., Lowry, K. E., and van Dijken, G. L.: Annual changes in sea ice and phytoplankton
926 in polynyas of the Amundsen Sea, Antarctica. *Deep-Sea Res. II.*, 71–76, 5–15.
927 <https://doi.org/10.1016/j.dsr2.2012.03.006>, 2012.

928 Arrigo, K. R., Robinson, D. H., Worthen, D. L., Dunbar, R. B., DiTullio, G. R., VanWoert, M.,
929 and Lizotte, M. P.: Phytoplankton community structure and the drawdown of nutrients and CO₂
930 in the Southern Ocean, *Sci*, 283, 5400, 365-367, DOI: 10.1126/science.283.5400.365, 1999.

931

932 Arrigo, K. R. and van Dijken, G. L.: Phytoplankton dynamics within 37 Antarctic coastal
933 polynya systems, *J. Geophys. Res. Ocean.*, 108, <https://doi.org/10.1029/2002JC001739>, 2003.

934 Arrigo, K. R., van Dijken, G. L., and Strong, A. L.: Environmental controls of marine
935 productivity hot spots around Antarctica, *J. Geophys. Res. Ocean.*, 120, 5545–5565,
936 <https://doi.org/10.1002/2015JC010888>, 2015.

937 Arrigo, K. R., Worthen, D., Schnell, A., and Lizotte, M. P.: Primary production in Southern
938 Ocean waters, *J. Geophys. Res. Ocean.*, 103, 15587–15600, <https://doi.org/10.1029/98JC00930>,
939 1998.

940 Assmann, K. M., Jenkins, A., Shoosmith, D. R., Walker, D., Jacobs, S., and and Nicholls, K.:
941 Variability of circumpolar deep water transport onto the Amundsen Sea continental shelf through
942 a shelf break trough. *J. Geophys. Res. Oceans*, 118, 6603–6620, doi:10.1002/2013JC008871,
943 2013.

944 Behrenfeld, M. J. and Falkowski, P. G.: Photosynthetic rates derived from satellite-based
945 chlorophyll concentration, *Limnol. Oceanogr.*, 42, 1–20,
946 <https://doi.org/10.4319/lo.1997.42.1.0001>, 1997.

947 Bett, D. T., Holland, P. R., Naveira Garabato, A. C., Jenkins, A., Dutrieux, P., Kimura, S., and
948 Fleming, A.: The Impact of the Amundsen Sea Freshwater Balance on Ocean Melting of the
949 West Antarctic Ice Sheet, *J. Geophys. Res. Oceans*, 125, <https://doi.org/10.1029/2020JC016305>,
950 2020.

951 Bhatia, M. P., Kujawinski, E. B., Das, S. B., Breier, C. F., Henderson, P. B., and Charette, M. A.:
952 Greenland meltwater as a significant and potentially bioavailable source of iron to the ocean,
953 *Nat. Geosci.*, 6, 274–278, <https://doi.org/10.1038/ngeo1746>, 2013.

954 Biddle, L. C., Heywood, K. J., Kaiser, J., and Jenkins, A.: Glacial Meltwater Identification in the
955 Amundsen Sea, *JPO*, 47, 933–954, <https://doi.org/10.1175/JPO-D-16-0221.1>, 2017.

956 Boles, E., Provost, C., Garçon, V., Bertosio, C., Athanase, M., Koenig, Z., and Sennéchael, N.:
957 Under-Ice Phytoplankton Blooms in the Central Arctic Ocean: Insights From the First
958 Biogeochemical IAOOS Platform Drift in 2017, *J. Geophys. Res. Ocean.*, 125, e2019JC015608,
959 <https://doi.org/10.1029/2019JC015608>, 2020.

960 Boyd, P. W., Jickells, T., Law, C. S., Blain, S., Boyle, E. A., Buesseler, K. O., Coale, K. H.,
961 Cullen, J. J., Baar, H. J. W. de, Follows, M., Harvey, M., Lancelot, C., Levasseur, M., Owens, N.
962 P. J., Pollard, R., Rivkin, R. B., Sarmiento, J., Schoemann, V., Smetacek, V., Takeda, S., Tsuda,
963 A., Turner, S., and Watson, A. J.: Mesoscale Iron Enrichment Experiments 1993-2005: Synthesis
964 and Future Directions, *Science*, 315, 612–617, <https://doi.org/10.1126/science.1131669>, 2007.

965 Cape, M. R., Vernet, M., Pettit, E. C., Wellner, J., Truffer, M., Akie, G., Domack, E., Leventer,
966 A., Smith, C. R., and Huber, B. A.: Circumpolar Deep Water Impacts Glacial Meltwater Export
967 and Coastal Biogeochemical Cycling Along the West Antarctic Peninsula, *Front. Mar. Sci.*, 6,
968 <https://doi.org/10.3389/fmars.2019.00144>, 2019.

969 Cavalieri, D., Parkinson, C., Gloersen, P., and Zwally, H. J.: Sea Ice Concentrations from
970 Nimbus-7 SMMR and DMSP SSM/I-SSMIS Passive Microwave Data, Version 1,
971 <https://doi.org/10.5067/8GQ8LZQVL0VL>, 1996.

972 Death, R., Wadham, J. L., Monteiro, F., Le Brocq, A. M., Tranter, M., Ridgwell, A., Dutkiewicz,
973 S., and Raiswell, R.: Antarctic ice sheet fertilises the Southern Ocean, *BG*, 11, 2635–2643,
974 <https://doi.org/10.5194/bg-11-2635-2014>, 2014.

975 Dinniman, M. S., St-Laurent, P., Arrigo, K. R., Hofmann, E. E., and Dijken, G. L.: Analysis of
976 Iron Sources in Antarctic Continental Shelf Waters, *J. Geophys. Res. Oceans.*, 125,
977 <https://doi.org/10.1029/2019JC015736>, 2020.

978 Dinniman, M. S., St-Laurent, P., Arrigo, K. R., Hofmann, E. E., and van Dijken, G. L.:
979 Sensitivity of the Relationship Between Antarctic Ice Shelves and Iron Supply to Projected
980 Changes in the Atmospheric Forcing, *J. Geophys. Res. Ocean.*, 128, e2022JC019210,
981 <https://doi.org/10.1029/2022JC019210>, 2023.

982 Dotto, T. S., Naveira Garabato, A. C., Bacon, S., Holland, P. R., Kimura, S., Firing, Y. L.,
983 Tsamados, M., Wåhlin, A. K., and Jenkins, A.: Wind-Driven Processes Controlling Oceanic
984 Heat Delivery to the Amundsen Sea, Antarctica, *J. Phys. Oceanogr.*, 49, 2829–2849,
985 <https://doi.org/10.1175/JPO-D-19-0064.1>, 2019.

986 Douglas, C. C., Briggs, N., Brown, P., MacGilchrist, G., and Naveira Garabato, A.: Exploring
987 the relationship between sea ice and phytoplankton growth in the Weddell Gyre using satellite
988 and Argo float data, *Ocean Sci.*, 20, 475–497, <https://doi.org/10.5194/os-20-475-2024>, 2024.
989

990 Dutrieux, P., De Rydt, J., Jenkins, A., Holland, P. R., Ha, H. K., Lee, S. H., Steig, E. J., Ding,
991 Q., Abrahamsen, E. P., and Schröder, M.: Strong sensitivity of Pine Island ice-shelf melting to
992 climate variability, *Sci*, 343, 6167, 174–178, DOI: 10.1126/science.1244341, 2014.
993

994 ECCO Consortium, Fukumori, I., Wang, O., Fenty, I., Forget, G., Heimbach, P., and Ponte, R.
995 M: ECCO Ocean Mixed Layer Depth - Monthly Mean 0.5 Degree 9Version 4 Release 4). ver
996 V4r4. PO.DACC, CA, USA, Dataset accessed [2025-08-22], <https://doi.org/10.5067/ECG5M-OML44>, 2021.
997

998 Forsch, K. O., Hahn-Woernle, L., Sherrell, R. M., Rocanova, V. J., Bu, K., Burdige, D., Vernet,
1000 M., and Barbeau, K. A.: Seasonal dispersal of fjord meltwaters as an important source of iron
1001 and manganese to coastal Antarctic phytoplankton, *Biogeo.*, 18, 6349–6375,
1002 <https://doi.org/10.5194/bg-18-6349-2021>, 2021.
1003

1004 Golder, M.R., and Antoine, D.: Physical drivers of long-term chlorophyll-a variability in the
1005 Southern Ocean, *Elem. Sci Anth*, 13:1, <https://doi.org/10.1525/elementa.2024.00077>, 2025.

1006
1007 Garabato, A. C. N., Forryan, A., Dutrieux, P., Brannigan, L., Biddle, L. C., Heywood, K. J.,
1008 Jenkins, A., Firing, Y. L., and Kimura, S.: Vigorous lateral export of the meltwater outflow from
1009 beneath an Antarctic ice shelf, *Nature*, 542, 219–222, <https://doi.org/10.1038/nature20825>, 2017.

1010 Gerringa, L. J. A., Alderkamp, A.-C., Laan, P., Thuróczy, C.-E., De Baar, H. J. W., Mills, M. M.,
1011 van Dijken, G. L., Haren, H. van, and Arrigo, K. R.: Iron from melting glaciers fuels the
1012 phytoplankton blooms in Amundsen Sea (Southern Ocean): Iron biogeochemistry, *Deep-Sea*
1013 *Res. II.*, 71–76, 16–31, <https://doi.org/10.1016/j.dsr2.2012.03.007>, 2012.

1014 Gerringa, L. J. A., Alderkamp, A.-C., Laan, P., Thuróczy, C.-E., de Baar, H. J. W., Mills, M. M.,
1015 van Dijken, G. L., van Haren, H., and Arrigo, K. R.: Corrigendum to “Iron from melting glaciers
1016 fuels the phytoplankton blooms in Amundsen Sea (Southern Ocean): iron biogeochemistry”
1017 (Gerringa et al., 2012), *Deep-Sea Res. II.*, 177, 104843,
1018 <https://doi.org/10.1016/j.dsr2.2020.104843>, 2020.

1019 Gledhill, M. and Buck, K.: The Organic Complexation of Iron in the Marine Environment: A
1020 Review, *Front. Microbiol.*, 3, <https://doi.org/10.3389/fmicb.2012.00069>. 2012.

1021 Goldberg, D. N., Twelves, A. G., Holland, P. R.. & Wearing, K. G.: The non-local impact of
1022 Antarctic subglacial runoff. *Journal of Geophysical Research: Oceans* 128, e2023JC019823.
1023 <https://doi.org/10.1029/2023JC019823>. 2023.

1024 Ha, H. K., Wåhlin, A. K., Kim, T. W., Lee, S. H., Lee, J. H., Lee, H. J., Hong, C. S., Arneborg,
1025 L., Björk, G., and Kalén, O.: Circulation and modification of warm deep water on the central
1026 Amundsen shelf, 44, 5, 1493–1501, <https://doi.org/10.1175/JPO-D-13-0240.1>, 2014.

1027
1028 Hassler, C., Cabanes, D., Blanco-Ameijeiras, S., Sander, S. G., Benner, R., Hassler, C., Cabanes,
1029 D., Blanco-Ameijeiras, S., Sander, S. G., and Benner, R.: Importance of refractory ligands and
1030 their photodegradation for iron oceanic inventories and cycling, *Mar. Fresh. Res.*, 71, 311–320,
1031 <https://doi.org/10.1071/MF19213>, 2019.

1032 Hawkings, J. R., Wadham, J. L., Tranter, M., Raiswell, R., Benning, L. G., Statham, P. J.,
1033 Tedstone, A., Nienow, P., Lee, K., and Telling, J.: Ice sheets as a significant source of highly
1034 reactive nanoparticulate iron to the oceans, *Nat. Commun.*, 5, 3929,
1035 <https://doi.org/10.1038/ncomms4929>, 2014.

1036 Hayward, A., Wright, S.W., Carroll, D. Law, C. S., Wongpan, P., Gutiérrez-Rodriguez, A., and
1037 Pinkerton, M. H.: Antarctic phytoplankton communities restructure under shifting sea-ice
1038 regimes. *Nat. Clim. Chang.* 15, 889–896, <https://doi.org/10.1038/s41558-025-02379-x>, 2025.

1039
1040 Herraiz-Borreguero, L., Lannuzel, D., van der Merwe, P., Treverrow, A., and Pedro, J. B.: Large
1041 flux of iron from the Amery Ice Shelf marine ice to Prydz Bay, East Antarctica, *J. Geophys. Res.*
1042 *Ocean.*, 121, 6009–6020, <https://doi.org/10.1002/2016JC011687>, 2016.

1043 Hersbach, H., Bell, B., Berrisford, P., Hirahara, S., Horányi, A., Muñoz-Sabater, J., Nicolas, J.,
1044 Peubey, C., Radu, R., Schepers, D., Simmons, A., Soci, C., Abdalla, S., Abellán, X., Balsamo,
1045 G., Bechtold, P., Biavati, G., Bidlot, J., Bonavita, M., De Chiara, G., Dahlgren, P., Dee, D.,

1046 Diamantakis, M., Dragani, R., Flemming, J., Forbes, R., Fuentes, M., Geer, A., Haimberger, L.,
1047 Healy, S., Hogan, R. J., Hólm, E., Janisková, M., Keeley, S., Laloyaux, P., Lopez, P., Lupu, C.,
1048 Radnoti, G., de Rosnay, P., Rozum, I., Vamborg, F., Villaume, S., and Thépaut, J.-N.: The ERA5
1049 global reanalysis, *Q. J. R. Meteorol. Soc.*, 146, 1999–2049, <https://doi.org/10.1002/qj.3803>,
1050 2020.

1051 Hosking, J. S., Orr, A., Marshall, G. J., Turner, J., and Phillips, T.: The Influence of the
1052 Amundsen–Bellingshausen Seas Low on the Climate of West Antarctica and Its Representation
1053 in Coupled Climate Model Simulations, *J. Clim.*, 26, 6633–6648, <https://doi.org/10.1175/JCLI-D-12-00813.1>, 2013.

1055 Hosking, J. S., Orr, A., Bracegirdle, T. J., and Turner, J.: Future circulation changes off West
1056 Antarctica: Sensitivity of the Amundsen Sea Low to projected anthropogenic forcing, *Geophys.*
1057 *Res. Lett.*, 43, 367–376, <https://doi.org/10.1002/2015GL067143>, 2016.

1058 Huang, B., Liu, C., Banzon, V., Freeman, E., Graham, G., Hankins, B., Smith, T., and Zhang,
1059 H.-M.: Improvements of the Daily Optimum Interpolation Sea Surface Temperature (DOISST)
1060 Version 2.1, *Journal of Climate*, 34, 2923–2939. doi: 10.1175/JCLI-D-20-0166.1, 2021.

1061

1062 Jacobs, S. S., Jenkins, A., Giulivi, C. F., and Dutrieux, P.: Stronger ocean circulation and
1063 increased melting under Pine Island Glacier ice shelf, *Nat. Geo.*, 4, 519–523,
1064 <https://doi.org/10.1038/ngeo1188>, 2011.

1065 Jena, B. and Pillai, A. N.: Satellite observations of unprecedented phytoplankton blooms in the
1066 Maud Rise polynya, Southern Ocean, *The Cryosphere*, 14, 1385–1398,
1067 <https://doi.org/10.5194/tc-14-1385-2020>, 2020.

1068

1069 Jenkins, A., Dutrieux, P., Jacobs, S. S., McPhail, S. D., Perrett, J. R., Webb, A. T., and White,
1070 D.: Observations beneath Pine Island glacier in West Antarctica and implications for its retreat,
1071 *Nat. Geo.*, 3, 468–472, <https://doi.org/10.1038/NGEO890>, 2010.

1072

1073 Jourdain, N. C., Mathiot, P., Merino, N., Durand, G., Le Sommer, J., Spence, P., Dutrieux, P.,
1074 and Madec, G.: Ocean circulation and sea-ice thinning induced by melting ice shelves in the
1075 Amundsen Sea, *J. Geophys. Res. Ocean.*, 122, 2550–2573,
1076 <https://doi.org/10.1002/2016JC012509>, 2017.

1077 Kauko, H. M., Hattermann, T., Ryan-Keogh, T., Singh, A., de Steur, L., Fransson, A., Chierici,
1078 M., Falkenhaug, T., Hallfredsson, E. H., Bratbak, G., Tsagaraki, T., Berge, T., Zhou, Q., and
1079 Moreau, S.: Phenology and Environmental Control of Phytoplankton Blooms in the Kong Håkon
1080 VII Hav in the Southern Ocean, *Front. Mar. Sci.*, 8, <https://doi.org/10.3389/fmars.2021.623856>,
1081 2021.

1082 Lannuzel, D., Fourquez, M., de Jong, J., Tison, J.-L., Delille, B., and Schoemann, V.: First report
1083 on biological iron uptake in the Antarctic sea-ice environment, *Polar Biol.*, 46, 339–355,
1084 <https://doi.org/10.1007/s00300-023-03127-7>, 2023.

1085 Lee, S. H., Kim, B. K., Lim, Y. J., Joo, H., Kang, J. J., Lee, D., Park, J., Ha, S.-Y., and Lee, S.
1086 H.: Small phytoplankton contribution to the standing stocks and the total primary production in
1087 the Amundsen Sea, *BG*, 14, 3705–3713, <https://doi.org/10.5194/bg-14-3705-2017>, 2017.

1088 Lee, Y., Park, J., Jung, J., and Kim, T. W.: Unprecedented differences in phytoplankton
1089 community structures in the Amundsen Sea polynyas, West Antarctica, *Environ. Res. Lett.* 17,
1090 114022, 10.1088/1748-9326/ac9a5f, 2022.

1091

1092 van Leeuwe, M. A., Webb, A. L., Venables, H. J., Visser, R. J. W., Meredith, M., P., Elzenga J.
1093 T. M., and Stefels, J.: Annual patterns in phytoplankton phenology in Antarctic coastal waters
1094 explained by environmental drivers, *Limnol. Oceanogr.*, 65, 1651–1668,
1095 <https://doi.org/10.1002/lno.11477>, 2020.

1096

1097 Liniger, G., Strutton, P. G., Lannuzel, D., and Moreau, S.: Calving event led to changes in
1098 phytoplankton bloom phenology in the Mertz polynya, Antarctica, *J. Geophys. Res. Oceans.*,
1099 125, e2020JC016387, <https://doi.org/10.1029/2020JC016387>, 2020.

1100

1101 Liu, Y., Moore, J. C., Cheng, X., Gladstone, R. M., Bassis, J. N., Liu, H., Wen, J., and Hui, F.:
1102 Ocean-driven thinning enhances iceberg calving and retreat of Antarctic ice shelves, *Proc. Nat.
1103 Acad. Sci.*, 112, 3263–3268, <https://doi.org/10.1073/pnas.1415137112>, 2015.

1104

1105 van Manen, M., Aoki, S., Brussaard, C. P. D., Conway, T. M., Eich, C., Gerringa, L., Jung, J.,
1106 Kim, T.-W., Lee, S. H., Lee, Y., Reichart, G.-J., Tian, H., Wille, F., and Middag, R.: The role of
1107 the Dotson Ice Shelf and circumpolar deep water as driver and source of dissolved and
1108 particulate iron and manganese in the Amundsen Sea polynya, Southern Ocean, *Mar. Chem.*,
1109 104161, <https://doi.org/10.1016/j.marchem.2022.104161>, 2022.

1110 Marchese, C., Albouy, C., Tremblay, J.-É., Dumont, D., D'Ortenzio, F., Vissault, S., and
1111 Bélanger, S.: Changes in phytoplankton bloom phenology over the North Water (NOW)
1112 polynya: a response to changing environmental conditions, *Polar Biol.*, 40, 1721–1737,
1113 <https://doi.org/10.1007/s00300-017-2095-2>, 2017.

1114 Maritorena, S., and Siegel, D. A.: Consistent merging of satellite ocean color data sets using a
1115 bio-optical model, *Rem. Sens. Environ.*, 94, 429–440, <https://doi.org/10.1016/j.rse.2004.08.014>,
1116 2005.

1117

1118 McClish, S., and Bushinsky, S. M.: Majority of Southern Ocean seasonal ice zone bloom net
1119 community production precedes total ice retreat, *Geophys. Res. Lett.*, 50, e2023GL103459.
1120 <https://doi.org/10.1029/2023GL103459>, 2023.

1121

1122 Meredith, M., Sommerkorn, M., Cassotta, S., Derksen, C., Ekaykin, A., Hollowed, A., Kofinas,
1123 G., Mackintosh, A., Melbourne-Thomas, J., Muelbert, M.M.C., Ottersen, G., Pritchard, H., and
1124 Schurr, E.A.G.: Polar Regions. In: *IPCC Special Report on the Ocean and Cryosphere in a
1125 Changing Climate* [H.-O. Pörtner, D.C. Roberts, V. Masson-Delmotte, P. Zhai, M. Tignor, E.
1126 Poloczanska, K. Mintenbeck, A. Alegría, M. Nicolai, A. Okem, J. Petzold, B. Rama, N.M.
1127 Weyer (eds.)]. Cambridge University Press, Cambridge, UK and New York, NY, USA, pp. 203–
1128 320, <https://doi.org/10.1017/9781009157964.005>, 2019.

1129 Mills, M. M., Lindsey, R.K., van Dijken, G. L., Alderkamp, C-A., Berg, G. M., Robinson, D. H.,
1130 Welschmeyer, N. A and Arrigo, K. R.: Photophysiology in two Southern Ocean phytoplankton
1131 taxa: photosynthesis of *phaeocystis antarctica* (prymnesiophyceae) and *fragiloriopsis cylindrus*
1132 (bacillariophyceae) under simulated mixed-layer irradiance, *J. Phycol.*, 46, 1114-1127,
1133 <https://doi.org/10.1111/j.1529-8817.2010.00923.x>, 2010.

1134 Mills, M. M., Alderkamp, C-A., Thuróczy, C-E., van Dijken, G. L., Laan, P., de Barr, H. J. W.
1135 and Arrigo, K. R.: Phytoplankton biomass and pigment responses to Fe amendments on the Pine
1136 Island and Amundsen polynyas, *Deep-Sea Res. II.*, 71-76, 61-76,
1137 <https://doi.org/10.1016/j.dsr2.2012.03.008>, 2012.

1138 Morales Maqueda, M. A.: Polynya Dynamics: a Review of Observations and Modeling, *Rev.
1139 Geophys.*, 42, RG1004, <https://doi.org/10.1029/2002RG000116>, 2004.

1140 Moreau, S., Mostajir, B., Bélanger, S., Schloss, I. R., Vancoppenolle, M., Demers, S., and
1141 Ferreyra, G. A.: Climate change enhances primary production in the western Antarctic Peninsula,
1142 *Global Change Biology*, 21, 2191–2205, <https://doi.org/10.1111/gcb.12878>, 2015.

1143 Naughten, K. A., Holland, P. R., and De Rydt, J.: Unavoidable future increase in West Antarctic
1144 ice-shelf melting over the twenty-first century, *Nat. Clim. Change.*, 13, 1222-1228,
1145 <https://doi.org/10.1038/s41558-023-01818-x>, 2023.

1146 Naughten, K. A., Meissner, K. J., Galton-Fenzi, B. K., England, M. H., Timmermann, R., and
1147 Hellmer, H. H.: Future Projections of Antarctic Ice Shelf Melting Based on CMIP5 Scenarios, *J.
1148 Clim.*, 31, 5243–5261, <https://doi.org/10.1175/JCLI-D-17-0854.1>, 2018.

1149 Nunes, G.S., Ferreira, A. and Brito, A.C. Long-term satellite data reveals complex phytoplankton
1150 dynamics in the Ross Sea, Antarctica. *Commun. Earth. Environ.*, 6, 864,
1151 <https://doi.org/10.1038/s43247-025-02590-w>, 2025.

1152
1153 Oh, J.-H., Noh, K. M., Lim, H.-G., Jin, E. K., Jun, S.-Y., and Kug, J.-S.: Antarctic meltwater-
1154 induced dynamical changes in phytoplankton in the Southern Ocean, *Environ. Res. Lett.*, 17,
1155 024022, <https://doi.org/10.1088/1748-9326/ac444e>, 2022.

1156 Oliver, H., St-Laurent, P., Sherrell, R. M., and Yager, P. L.: Modeling Iron and Light Controls
1157 on the Summer *Phaeocystis antarctica* Bloom in the Amundsen Sea Polynya, *Global
1158 Biogeochem. Cycles*, 2018GB006168, <https://doi.org/10.1029/2018GB006168>, 2019.

1159 Pan, J. B., Gierach, M. M., Stammerjohn, S., Schofield, O., Meredith, M. P., Reynolds, R. A.,
1160 vernet, M., Haumann, F. A., Orona, A. J., and Miller, C. E.: Impact of glacial meltwater on
1161 phytoplankton biomass along the Western Antarctic Peninsula. *Comm. Earth. Environ.*, 6(456).
1162 <https://doi.org/10.1038/s43247-025-02435-6>. 2025

1163 Paolo, F. S., Fricker, H. A., and Padman, L.: Volume loss from Antarctic ice shelves is
1164 accelerating, *Science*, 348, 327–331, <https://doi.org/10.1126/science.aaa0940>, 2015.

1165 Paolo, F. S., Fricker, H. A., and Padman, L.: Constructing improved decadal records of Antarctic
1166 ice shelf height change from multiple satellite radar altimeters, *Remote Sens. Environ.* 177, 192–
1167 205, <https://doi.org/10.1016/j.rse.2016.01.026>, 2016.

1168 Paolo, F. S., Gardner, A. S., Greene, C. A., Nilsson, J., Schodlok, M. P., Schlegel, N.-J., and
1169 Fricker, H. A.: Widespread slowdown in thinning rates of West Antarctic ice shelves, *TC*, 17,
1170 3409–3433, <https://doi.org/10.5194/tc-17-3409-2023>, 2023.

1171 Park, J., Kuzminov, F. I., Bailleul, B., Yang, E. J., Lee, S., Falkowski, P. G., and Gorbunov, M.
1172 Y.: Light availability rather than Fe controls the magnitude of massive phytoplankton bloom in
1173 the Amundsen Sea polynyas, Antarctica: Light availability rather than Fe controls phytoplankton
1174 bloom, *Limnol. Oceanogr.*, 62, 2260–2276, <https://doi.org/10.1002/lo.10565>, 2017.

1175 Park, J., Kim, J.-H., Kim, H., Hwang, J., Jo, Y.-H., and Lee, S. H.: Environmental Forcings on
1176 the Remotely Sensed Phytoplankton Bloom Phenology in the Central Ross Sea Polynya, *J.*
1177 *Geophys. Res. Ocean.*, 124, 5400–5417, <https://doi.org/10.1029/2019JC015222>, 2019.

1178 Person, R., Aumont, O., Madec, G., Vancoppenolle, M., Bopp, L., and Merino, N.: Sensitivity of
1179 ocean biogeochemistry to the iron supply from the Antarctic Ice Sheet explored with a
1180 biogeochemical model, *BG*, 16, 3583–3603, <https://doi.org/10.5194/bg-16-3583-2019>, 2019.

1181 Pritchard, H. D., Ligtenberg, S. R. M., Fricker, H. A., Vaughan, D. G., van den Broeke, M. R.,
1182 and Padman, L.: Antarctic ice-sheet loss driven by basal melting of ice shelves, *Nat.*, 484, 502–
1183 505, <https://doi.org/10.1038/nature10968>, 2012.

1184 Racault, M.-F., Le Quéré, C., Buitenhuis, E., Sathyendranath, S., and Platt, T.: Phytoplankton
1185 phenology in the global ocean, *Ecol. Indic.*, 14, 152–163,
1186 <https://doi.org/10.1016/j.ecolind.2011.07.010>, 2012.

1187 Randall-Goodwin, E., Meredith, M. P., Jenkins, A., Yager, P. L., Sherrell, R. M., Abrahamsen,
1188 E. P., Guerrero, R., Yuan, X., Mortlock, R. A., Gavahan, K., Alderkamp, A.-C., Ducklow, H.,
1189 Robertson, R., and Stammerjohn, S. E.: Freshwater distributions and water mass structure in the
1190 Amundsen Sea Polynya region, Antarctica, *Elem. Sci. Anth.*, 3, 000065,
1191 <https://doi.org/10.12952/journal.elementa.000065>, 2015.

1192 Rignot, E., Jacobs, S., Mouginot, J., and Scheuchl, B.: Ice-Shelf Melting Around Antarctica, *Sci.*
1193 341, 266–270, <https://doi.org/10.1126/science.1235798>, 2013.

1194 Rignot, E., Mouginot, J., Scheuchl, B., van den Broeke, M., van Wessem, M. J., and Morlighem,
1195 M.: Four decades of Antarctic Ice Sheet mass balance from 1979–2017, *Proc. Nat. Acad. Sci.*,
1196 116, 4, 1095–1103, <https://doi.org/10.1073/pnas.1812883116>, 2019.

1197 Ryan-Keogh, T. J., Thomalla, S. J., Chang, N., and Moalusi, T.: A new global oceanic multi-
1198 model net primary productivity data product, *Earth Syst. Sci. Data*, 15, 4829–4848,
1199 <https://doi.org/10.5194/essd-15-4829-2023>, 2023.

1200
1201 Sari El Dine, Z., Guinet, C., Picard, B., Thyssen, M., Duforêt-gaurier, L., and El Hourany,
1202 R.: Influence of the phytoplankton community structure on the southern elephant seals' foraging

1203 activity within the Southern Ocean, *Commun. Biol.*, 8, 620, <https://doi.org/10.1038/s42003-025-08049-0>, 2025.

1204

1205

1206 Scambos, T., Bell, R. E., Alley, R. B., Anandakrishnan, S., Bromwich, D. H., Brunt, K.,
1207 Christianson, K., Creyts, T., Das, S. B., DeConto, R., Dutrieux, P., Fricker, H. A., Holland, D.,
1208 MacGregor, J., Medley, B., Nicolas, J. P., Pollard, D., Siegfried, M. R., Smith, A. M., Steig, E.
1209 J., Trusel, L. D., Vaughan, D. G., and Yager, P. L.: How much, how fast?: A science review and
1210 outlook for research on the instability of Antarctica's Thwaites Glacier in the 21st century, *Glob.*
1211 *Planet. Change.*, 153, 16-34, <https://doi.org/10.1016/j.gloplacha.2017.04.008>, 2017.

1212

1213 Silsbe, G. M., Behrenfeld, M. J., Halsey, K. H., Milligan, A. J., and Westberry, T. K.: The CAFE
1214 model: A net production model for global ocean phytoplankton, *Global Biogeochem. Cycles.*,
1215 30, 1756–1777, doi:10.1002/2016GB005521, 2016.

1216 Shepherd, A., Ivins, E., Rignot, E., Smith, B., van den Broeke, M., Velicogna, I., Whitehouse, P.,
1217 Briggs, K., Joughin, I., Krinner, G., Nowicki, S., Payne, T., Scambos, T., Schlegel, N., A. G.,
1218 Agosta, C., Ahlstrøm, A., Babonis, G., Barletta, V., Blazquez, A., Bonin, J., Csatho, B.,
1219 Cullather, R., Felikson, D., Fettweis, X., Forsberg, R., Gallee, H., Gardner, A., Gilbert, L., Groh,
1220 A., Gunter, B., Hanna, E., Harig, C., Helm, V., Horvath, A., Horwath, M., Khan, S., Kjeldsen, K.
1221 K., Konrad, H., Langen, P., Lecavalier, B., Loomis, B., Luthcke, S., McMillan, M., Melini, D.,
1222 Mernild, S., Mohajerani, Y., Moore, P., Mouginot, J., Moyano, G., Muir, A., Nagler, T., Nield,
1223 G., Nilsson, J., Noel, B., Otosaka, I., Pattle, M. E., Peltier, W. R., Pie, N., Rietbroek, R., Rott, H.,
1224 Sandberg-Sørensen, L., Sasgen, I., Save, H., Scheuchl, B., Schrama, E., Schröder, L., Seo, K.-
1225 W., Simonsen, S., Slater, T., Spada, G., Sutterley, T., Talpe, M., Tarasov, L., van de Berg, W. J.,
1226 van der Wal, W., van Wessem, M., Vishwakarma, B. D., Wiese, D., Wouters, B., and The
1227 IMBIE team: Mass balance of the Antarctic Ice Sheet from 1992 to 2017, *Nat.*, 558, 219–222,
1228 <https://doi.org/10.1038/s41586-018-0179-y>, 2018.

1229 Sherrell, R. M., Lagerström, M. E., Forsch, K. O., Stammerjohn, S. E., and Yager, P. L.:
1230 Dynamics of dissolved iron and other bioactive trace metals (Mn, Ni, Cu, Zn) in the Amundsen
1231 Sea Polynya, Antarctica, *Elementa: Sci. Anthrop.*, 3, 000071,
1232 <https://doi.org/10.12952/journal.elementa.000071>, 2015.

1233 Siegel, D. A., Doney, S. C., and Yoder, J. A.: The North Atlantic Spring Phytoplankton Bloom
1234 and Sverdrup's Critical Depth Hypothesis, *Science*, 296, 730–733,
1235 <https://doi.org/10.1126/science.1069174>, 2002.

1236 Smith, A. J. R., Nelson, T., Ratnarajah, L., Genovese, C., Westwood, K., Holmes, T. M., Corkill,
1237 M., Townsend, A. T., Bell, E., Wuttig, K., and Lannuzel, D.: Identifying potential sources of
1238 iron-binding ligands in coastal Antarctic environments and the wider Southern Ocean, *Front. Mar. Sci.*, 9, <https://doi.org/10.3389/fmars.2022.948772>, 2022.

1240 Soppa, M. A., Völker, C., and Bracher, A.: Diatom Phenology in the Southern Ocean: Mean
1241 Patterns, Trends and the Role of Climate Oscillations, *Remote Sens.*, 8, 420,
1242 <https://doi.org/10.3390/rs8050420>, 2016.

1243 Stammerjohn, S. E., Martinson, D. G., Smith, R. C., and Iannuzzi, R. A.: Sea ice in the western
1244 Antarctic Peninsula region: Spatio-temporal variability from ecological and climate change
1245 perspectives, *Deep-Sea Res. II.*, 55, 2041–2058, <https://doi.org/10.1016/j.dsr2.2008.04.026>,
1246 2008.

1247 Stoer, A. C., and Fennel, K.: Carbon-centric dynamics of Earth's marine phytoplankton, *Proc.
1248 Nat. Acad. Sci.*, 121, 45, e2405354121, <https://doi.org/10.1073/pnas.2405354121>
1249 , 2024.

1250

1251 St-Laurent, P., Yager, P. L., Sherrell, R. M., Stammerjohn, S. E., and Dinniman, M. S.: Pathways
1252 and supply of dissolved iron in the Amundsen Sea (Antarctica), *J. Geophys. Res. Oceans.*, 122,
1253 7135–7162, <https://doi.org/10.1002/2017JC013162>, 2017.

1254 St-Laurent, P., Yager, P. L., Sherrell, R. M., Oliver, H., Dinniman, M. S., and Stammerjohn, S.
1255 E.: Modeling the Seasonal Cycle of Iron and Carbon Fluxes in the Amundsen Sea Polynya,
1256 Antarctica, *J. Geophys. Res. Oceans.*, 124, 1544–1565, <https://doi.org/10.1029/2018JC014773>,
1257 2019.

1258 Tagliabue, A., Bowie, A. R., DeVries, T., Ellwood, M. J., Landing, W. M., Milne, A., Ohnemus,
1259 D. C., Twining, B. S., and Boyd, P. W.: The interplay between regeneration and scavenging
1260 fluxes drives ocean iron cycling, *Nat Commun.*, 10, 4960, [https://doi.org/10.1038/s41467-019-12775-5](https://doi.org/10.1038/s41467-019-
1261 12775-5), 2019.

1262 Tamsitt, V., England, M. H., Rintoul, S. R., and Morrison, A. K.: Residence Time and
1263 Transformation of Warm Circumpolar Deep Water on the Antarctic Continental Shelf, *Geophys.
1264 Res. Lett.*, 48, e2021GL096092, <https://doi.org/10.1029/2021GL096092>, 2021.

1265 Tamura, T. P., Nomura, D., Hirano, D., Tamura, T., Kiuchi, M., Hashida, G., Makabe, R., Ono,
1266 K., Ushio, S., Yamazaki, K., Nakayama, Y., Takahashi, K. D., Sasaki, H., Murase, H., and Aoki,
1267 S.: Impacts of basal melting of the Totten Ice Shelf and biological productivity on marine
1268 biogeochemical components in Sabrina Coast, East Antarctica, *Global Biogeochem. Cycles.*, 37,
1269 e2022GB007510, <https://doi.org/10.1029/2022GB007510>, 2023.

1270 Thomalla, S.J., Nicholson, S.A., Ryan-Keogh, T.J. *et al.* Widespread changes in Southern Ocean
1271 phytoplankton blooms linked to climate drivers. *Nat. Clim. Chang.* 13, 975–984,
1272 <https://doi.org/10.1038/s41558-023-01768-4>, 2023.

1273 Thuróczy, C.-E., Alderkamp, A.-C., Laan, P., Gerringa, L. J. A., Mills, M. M., van Dijken, G. L.,
1274 De Baar, H. J. W., and Arrigo, K. R.: Key role of organic complexation of iron in sustaining
1275 phytoplankton blooms in the Pine Island and Amundsen Polynyas (Southern Ocean), *Deep-Sea
1276 Res. II.*, 71–76, 49–60, <https://doi.org/10.1016/j.dsr2.2012.03.009>, 2012.

1277 Turner, J., Hosking, J. S., Marshall, G. J., Phillips, T., and Bracegirdle, T. J.: Antarctic sea ice
1278 increase consistent with intrinsic variability of the Amundsen Sea Low, *Clim. Dyn.*, 46, 2391–
1279 2402, <https://doi.org/10.1007/s00382-015-2708-9>, 2016.

1280 Twelves, A. G., Goldberg, D. N., Henley, S. F., Mazloff, M. R. and Jones, D. C.: Self-shading
1281 and meltwater spreading control the transition from light to iron limitation in an Antarctic coastal

1282 polynya, *J. Geophys. Res. Oceans.*, 126, e2020JC016636,
1283 <https://doi.org/10.1029/2020JC016636>, 2021.

1284

1285 Vaillancourt, R. D., Sambrotto, R. N., Green, S., and Matsuda, A.: Phytoplankton biomass and
1286 photosynthetic competency in the summertime Mertz Glacier Region of East Antarctica, *Deep-*
1287 *Sea Res.* II., 50, 1415–1440, [https://doi.org/10.1016/S0967-0645\(03\)00077-8](https://doi.org/10.1016/S0967-0645(03)00077-8), 2003.

1288

1289 Westberry, T., Behrenfeld, M. J., Siegel, D. A., and Boss, E.: Carbon-based primary productivity
1290 modeling with vertically resolved photoacclimation, *Global Biogeoch. Cycle.*, 22, GB2024,
1291 doi:10.1029/2007GB003078, 2008.

1292

1293 Yager, P. L., Sherrell, R. M, Stammerjohn, S., Alderkamp, A.-C., Schofield, O., Abrahamsen, P.,
1294 Arrigo, K., Bertilsson, S., Garay, L., Guerrero, R., Lowry, K., Moksnes, P.-O., Ndungo, K., Post,
1295 A., Randall-Goodwin, E., Riemann, L., Severmann, S., Thatje, S., van Dijken, G., and Wilson,
1296 S.: ASPIRE: The Amundsen Sea Polynya International Research Expedition, *Oceanog.*, 25, 40–
53, <https://doi.org/10.5670/oceanog.2012.73>, 2012.

1297

1298 Yager P. L, Sherrell, R.M., Stammerjohn, S.E., Ducklow, H. W., Schofield, O., Ingall E.D.,
1299 Wilson, S. E., Lowry, K. E., Willismd, C. M., Riemman, L., Bertilsson, S., Alderkamp, A-C.,
1300 Dinasquet, J., Logares, R., Richert, I., Sipler, R. E., Melara A. J., Mu, L., Newstead, R. G., Post,
1301 A. F., Swalethorp, R and van Dijken, G. L.: A carbon budget for the Amundsen Sea Polynya,
1302 Antarctica: Estimating net community production and export in a highly productive polar
ecosystem, *Elem. Sci. Anth.*, 4, 000140, doi: 10.12952/journal.elementa.000140, 2016.

1303

1304 Yu, L.-S., He, H., Leng, H., Liu, H., and Lin, P.: Interannual variation of summer sea surface
1305 temperature in the Amundsen Sea, Antarctica, *Front. Mar. Sci.*, 10,
<https://doi.org/10.3389/fmars.2023.1050955>, 2023.

1306

1307 Zheng, Y., Heywood, K. J., Webber, B. G. M., Stevens, D. P., Biddle, L. C., Boehme, L., and
1308 Loose, B.: Winter seal-based observations reveal glacial meltwater surfacing in the southeastern
1309 Amundsen Sea, *Commun. Earth. Environ.*, 2, 1–9, <https://doi.org/10.1038/s43247-021-00111-z>,
2021.

1310